Spin polarized transport in low dimensional systems

Moumita Dey[†], **Santanu K. Maiti**[†,‡,*] **and S. N. Karmakar**[†]

[†] *Theoretical Condensed Matter Physics Division*
Saha Institute of Nuclear Physics
1/AF, Bidhannagar, Kolkata-700 064, India

[‡] *Department of Physics*
Narasinha Dutt College
129, Belilious Road, Howrah-711 101, India

[*] **Electronic mail**: santanu.maiti@saha.ac.in

Contents

1 Introduction

In the modern age of nanoscience and technology, spin dependent electron transport has opened a new branch both in theoretical and experimental Condensed Matter Physics, the so-called Spintronics. The word spintronics (spin transport electronics) was originated in 1994 during the manifestation of a new electronic device based on the role of the spin of the carriers, instead of or in addition to their charge. The advanced technological progress in fabrication and characterization of hybrid nanostructures has enabled us to study the spin dependent transport in low-dimensional systems like quantum wires, quantum dots, array of quantum dots, etc., in a very tunable environment.

For modeling and building spin based electronic devices, a clear understanding of spin dependent transport through hetero-interfaces is needed. Presently, spintronic devices are manufactured with the aid of two different approaches. The first approach is associated with the developing of the existing giant-magnetoresistance (GMR)-based technology. A giant-magnetoresistive sandwich structure is a prototype device which has widespread application in industry as a read head and a memory-storage cell. This structure consists of alternating ferromagnetic and nonmagnetic metallic layers, and, changing the relative orientation of the magnetization vectors in different magnetic layers one can tune the device resistance from the very low value to a very large one. This phenomenon can be utilized to sense changes in magnetic fields. The second approach searches novel techniques for generation as well as utilization of spin-polarized currents. The investigation of spin transport in semiconducting heterostructures is a major challenge to us, and, people are searching the ways in which these systems can act as spin polarizers and spin valves. The reason is that the existing metal-based devices cannot amplify signals, while semiconductor-based spintronic devices can in principle provide amplification and serve as multi-functional devices. Not only that, the semiconductor-based devices can be integrated much easily with the traditional semiconductor technology.

At present the generation of spin polarized electron beam and its transmission through matter is one of the most promising research topics in spintronics. At the same footing, several other phenomena have to be explored to develop the spin dependent transport. For our illustrative purposes, here we mention some of them as follow. In metals, the excitation as well as the switching of magnetization with the help of spin torques is an important issue. The spin dependent transport in metal-semiconductor interface, the spin tunneling through insulators, semiconducting heterostructures, etc., also draw much attention in this particular field. All these studies may be helpful for the development of quantum information processing and quantum computation.

In addition to the spin dependent transport measurements, the studies of spin polarized beam support an interesting model, the so-called 'two current model', which can be used for those electrons having kinetic energies ranging from diffusive to ballistic regime. The model illustrates that, electrons with up and down spins form two different current carrying channels,

associated with the different resistivities. This phenomenon provides dramatic effects, when the magnetization changes abruptly at the interface between two magnetically distinct materials. As representative examples: GMR Effect, TMR Effect (tunnel-magnetoresistance), Spin Torque effect during spin injection and spin transport across metal-semiconductor interfaces. Let us now concentrate our study on the generation of spin polarized electron beams.

2 Generation of spin polarized electron beams

2.1 Separation of electronic spin states

To reveal the interaction of spin polarized electrons with matter, we need a source of spin polarized electrons [1]. In the pioneer experiment of Stern and Gerlach, the two spin states of the unpaired valence electron of the charge neutral Ag atom were separated by applying an inhomogeneous magnetic field. However, for a free electron there is no such method which can separate the two spin states by applying an external magnetic field. This is due to the overwhelming effect of the Lorentz force acting on the charge of moving electrons.

It is well known that ferromagnets are the natural sources of polarized electrons, and one can extract the polarized electrons using photo emission technique or through proper tunneling method. But, there are some disadvantages for the ferromagnetic sources, since to switch over the spin direction, the inversion of the magnetization of the cathode is needed. This can make a trouble in emerging electron beam due to the existence of the residual stray magnetic fields at the ferromagnetic cathode.

In the present age, the widely used source of polarized electron is the Ga-As type semiconductors, where electrons are extracted through photo emission. Though Ga-As is a nonmagnetic semiconductor, but a large amount of spin polarized electrons can be extracted with the aid of a circularly polarized infra-red radiation.

2.2 Ga-As semiconductor as a polarized electron source

Here we explore how a Ga-As semiconductor can be used as a source of polarized electrons. In Ga-As material, the electrons at the top of the completely filled valance band are localized between the As atomic sites ($Z = 33$) and the electrons at the bottom of the conduction band are localized on the sites of Ga atoms ($Z = 31$). Accordingly, the electrons can undergo direct vertical transitions from the top of the valance band to the bottom of the conduction band.

The actual mechanism of getting spin polarized electrons from Ga-As source is schematically shown in Fig. 1. The valance band of the Ga-As semiconductor is made up of 4p atomic orbitals of As atoms those are splitted by spin orbit (SO) interaction into $4p_{1/2}$ and $4p_{3/2}$ states with an energy separation ~ 0.34 eV. $4p_{1/2}$ state is not shown here in the figure (Fig. 1). On the other hand, the conduction band is composed of 4s atomic orbitals of Ga atoms giving rise to a $4s_{1/2}$

state. By choosing the photon energy ~ 1.5 eV ($\sim$ band gap energy), higher energy transition i.e., the transition from the state $4p_{1/2}$ to the state $4s_{1/2}$ can be blocked.

Due to the existence of the cubic crystalline symmetry in the electric field, the $4p_{3/2}$ state is four-fold degenerate in energy. The conservation of angular momentum in the absorption of circularly polarized light provides $\Delta m_j = \pm 1$ for the allowed transitions. With the help of left circularly polarized (LCP) light, transitions with $\Delta m_j = -1$ are allowed only, while, for the transitions with $\Delta m_j = +1$, the right circularly polarized (RCP) light is needed. Thus, in cubic Ga-As only the transitions (I) $4p_{3/2}(m_j = +3/2) \rightarrow 4s_{1/2}(m_j = +1/2)$ and (II) $4p_{3/2}(m_j = 1/2) \rightarrow 4s_{1/2}(m_j = -1/2)$ can occur with the help of LCP light, obeying the selection rule $\Delta m_j = -1$. A similar type of transitions also take place from the other two states in the valance band to the two states in the conduction band by using the RCP light, following the selection rule $\Delta m_j = +1$. Therefore, both the spin states will be present in the conduction band. But, the

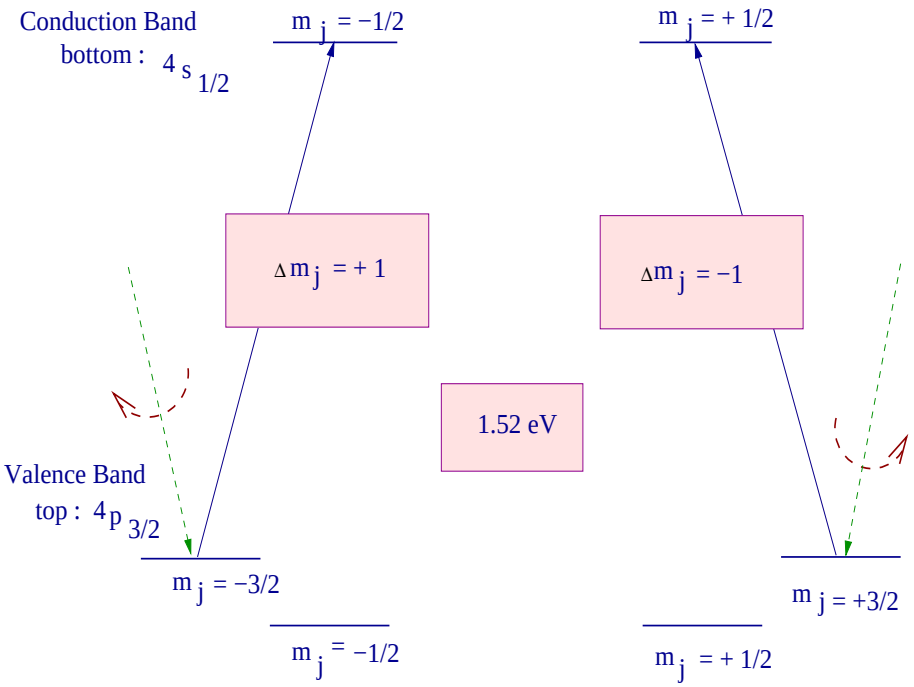

Figure 1: Optical spin orientation induced by transitions across the band gap in a Ga-As semiconductor.

transition probability of (I) is three times larger than the transition probability of (II). Hence, in the undistorted cubic Ga-As, the degree of spin polarization becomes,

$$P = \frac{3-1}{3+1} = 0.5 = 50\ \% \tag{1}$$

The degree of spin polarization can be made 100% with a slight modification in the Ga-As material. The spherical symmetry of the crystal field can be destroyed by distorting the cubic crystalline symmetry in the electric field of Ga-As through epitaxial growth on a lattice mis-

matched substrate, and accordingly, the energy levels get splitted with $m_j = \pm 3/2$ having a higher energy ~ 0.1 eV than $m_j = \pm 1/2$ (see Fig. 1). By tuning the photon energy to the edge of the band gap, fully polarized spin up or spin down electrons can be produced in the conduction band by simply switching between LCP and RCP lights.

Here it is important to note that, the surface of the Ga-As material can be made with negative electron affinity. It manifests that the electrons at the bottom of the conduction band can escape into vacuum without any additional supply of energy.

3 Formal description of spin polarized electrons

3.1 Quantum behavior of a single spin

According to the fundamental postulate of quantum mechanics, a wave function $\psi(\vec{r}, t)$ associated with a microscopic particle having linear momentum $\vec{p}$ and energy E can be expressed as,

$$\psi(\vec{r}, t) = A\ e^{i(\vec{k}.\vec{r} - \omega t)} \tag{2}$$

where A being a constant.
ω and $\vec{k}$ satisfy the following relations,

$$\hbar\omega = E \tag{3}$$

and,

$$\hbar\vec{k} = \vec{p} \tag{4}$$

The phase velocity of the wave packet is ω/k.

Since we are dealing with non-relativistic electrons, the space and spin parts of the wave function can be written separately. Thus we can write,

$$\psi(\vec{r}, t, s) = \chi(s)\ A\ e^{i(\vec{k}.\vec{r} - \omega t)} \tag{5}$$

Due to the presence of a magnetic field or an effective magnetic field, if there exists an energy difference between the two spin states of an electron i.e., $\Delta E\,(= E_\uparrow - E_\downarrow) \neq 0$, then the two spin states will travel with distinct phase velocities.

In the forthcoming two subsections (3.2 and 3.3), we discuss the behavior of a single spin polarized electron and an ensemble of spin polarized electrons, the so-called a spin polarized electron beam. A spin polarization vector $\vec{P}$ is introduced for the description of a spin polarized beam, where its component P_ξ for the quantization direction ξ is determined by the number of up ($\uparrow$) and down ($\downarrow$) spins along ξ. For the complete specification of a spin polarized electron beam, the polarization vector $\vec{P}$ as well as the number of electrons has to be specified.

To be precise, the main goal of studying a spin polarized electron beam is to answer a fundamental question, which is, "If a beam of n spin polarized electrons described by a polarization

vector $\vec{P}$, traverses through a sample of magnetization $\vec{M}$ which is oriented at an arbitrary angle with respect to $\vec{P}$, what will be the magnitude and direction of $\vec{P}$, when the electron beam will emerge from the sample ?"

3.2 Single electron polarization in Pauli spin formulation

Let us start with the basis vectors in σ_z diagonal representation, viz,

$$\chi_{up} = |\uparrow\rangle \equiv \begin{pmatrix} 1 \\ 0 \end{pmatrix} \tag{6}$$

$$\chi_{down} = |\downarrow\rangle \equiv \begin{pmatrix} 0 \\ 1 \end{pmatrix} \tag{7}$$

For an electron with spin in arbitrary direction, the spin part of the wave function can be written as,

$$\chi = \begin{pmatrix} u_1 \\ u_2 \end{pmatrix} \tag{8}$$

$$\Rightarrow \chi = u_1 \begin{pmatrix} 1 \\ 0 \end{pmatrix} + u_2 \begin{pmatrix} 0 \\ 1 \end{pmatrix} \tag{9}$$

where, u_1 and u_2 being arbitrary complex numbers.
By definition,

$$\chi^* = \begin{pmatrix} u_1^* & u_2^* \end{pmatrix} \tag{10}$$

Using the normalization condition $\chi^*\chi = 1$, we get,

$$u_1^* u_1 + u_2^* u_2 = 1 \tag{11}$$

This is just the one constraint, there are still three free choices of parameters for the determination of u_1 and u_2, since these are the complex numbers.
Expectation values of spin components along x, y and z axes are given by $\langle\sigma_x\rangle$, $\langle\sigma_y\rangle$ and $\langle\sigma_z\rangle$, respectively, where the components are,

$$\sigma_x = \begin{pmatrix} 0 & 1 \\ 1 & 0 \end{pmatrix}; \quad \sigma_y = \begin{pmatrix} 0 & -i \\ i & 0 \end{pmatrix}; \quad \sigma_z = \begin{pmatrix} 1 & 0 \\ 0 & -1 \end{pmatrix} \tag{12}$$

These are the so-called Pauli spin matrices. Now considering the general spin wave function χ, the expectation values of the Pauli matrices are as follow:

$$\begin{aligned} \langle\sigma_x\rangle &= \langle\chi|\sigma_x|\chi\rangle \\ &= u_1^* u_2 + u_2^* u_1 \end{aligned} \tag{13}$$

$$\begin{aligned}\langle\sigma_y\rangle &= \langle\chi|\sigma_y|\chi\rangle \\ &= i[u_2^* u_1 - u_1^* u_2] \end{aligned} \tag{14}$$

$$\begin{aligned}\langle\sigma_z\rangle &= \langle\chi|\sigma_z|\chi\rangle \\ &= u_1^* u_1 - u_2^* u_2 \end{aligned} \tag{15}$$

The polarization vector $\vec{P}$ of a single spin is defined as,

$$\vec{P} = \begin{pmatrix} P_x \\ P_y \\ P_z \end{pmatrix} \equiv \begin{pmatrix} \langle\sigma_x\rangle \\ \langle\sigma_y\rangle \\ \langle\sigma_z\rangle \end{pmatrix} \tag{16}$$

Therefore, using the Eqs. (13), (14) and (15), the polarization vector $\vec{P}$ can be written as,

$$\vec{P} = \begin{pmatrix} P_x \\ P_y \\ P_z \end{pmatrix} \equiv \begin{pmatrix} (u_1^* u_2 + u_2^* u_1) \\ i(u_2^* u_1 - u_1^* u_2) \\ (u_1^* u_1 - u_2^* u_2) \end{pmatrix} \tag{17}$$

Thus, depending on the choices of χ, the polarization $\vec{P}$ will have some specific forms. For illustrative purposes here we set few examples.

Case 1: The spin is directed along $+X$ axis.
For this particular choice, we can write,

$$\chi = \frac{1}{\sqrt{2}} \begin{pmatrix} 1 \\ 1 \end{pmatrix} \tag{18}$$

Using this expression of χ, the expectation values of the Pauli spin matrices are,

$$\langle\sigma_x\rangle = 1, \qquad \langle\sigma_y\rangle = 0, \qquad \langle\sigma_z\rangle = 0 \tag{19}$$

So the polarization vector $\vec{P}$ becomes,

$$\vec{P} \equiv \begin{pmatrix} P_x \\ P_y \\ P_z \end{pmatrix} = \begin{pmatrix} 1 \\ 0 \\ 0 \end{pmatrix} \tag{20}$$

Case 2: The spin is directed along $-X$ axis.
For this specific case the wave function can be chosen as,

$$\chi = \frac{1}{\sqrt{2}} \begin{pmatrix} 1 \\ -1 \end{pmatrix} \tag{21}$$

With this form of χ, we get,

$$\langle \sigma_x \rangle = -1, \qquad \langle \sigma_y \rangle = 0, \qquad \langle \sigma_z \rangle = 0 \tag{22}$$

Therefore, the polarization vector $\vec{P}$ becomes,

$$\vec{P} \equiv \begin{pmatrix} P_x \\ P_y \\ P_z \end{pmatrix} = \begin{pmatrix} -1 \\ 0 \\ 0 \end{pmatrix} \tag{23}$$

In a similar way, we also get the polarization vector ($\vec{P}$) when the spin is aligned in other directions. For representative examples, the results are summarized in Table 1.

Table 1: Spin wave function and polarization vector for spin alignments along X, Y and Z axes.

Spin alignment	Spin wave function	Polarization vector
Along + X axis	$\frac{1}{\sqrt{2}} \begin{pmatrix} 1 \\ 1 \end{pmatrix}$	$\begin{pmatrix} 1 \\ 0 \\ 0 \end{pmatrix}$
Along − X axis	$\frac{1}{\sqrt{2}} \begin{pmatrix} 1 \\ -1 \end{pmatrix}$	$\begin{pmatrix} -1 \\ 0 \\ 0 \end{pmatrix}$
Along + Y axis	$\frac{1}{\sqrt{2}} \begin{pmatrix} 1 \\ i \end{pmatrix}$	$\begin{pmatrix} 0 \\ 1 \\ 0 \end{pmatrix}$
Along − Y axis	$\frac{1}{\sqrt{2}} \begin{pmatrix} 1 \\ -i \end{pmatrix}$	$\begin{pmatrix} 0 \\ -1 \\ 0 \end{pmatrix}$
Along + Z axis	$\begin{pmatrix} 1 \\ 0 \end{pmatrix}$	$\begin{pmatrix} 0 \\ 0 \\ 1 \end{pmatrix}$
Along − Z axis	$\begin{pmatrix} 0 \\ 1 \end{pmatrix}$	$\begin{pmatrix} 0 \\ 0 \\ -1 \end{pmatrix}$

Determination of the complex coefficients u_1 and u_2

The complex coefficients u_1 and u_2 can be derived, in general, if the polarization vector $\vec{P}$ is given. The vector $\vec{P}$ can have any arbitrary direction in space. The factors $|u_1|^2$ and $|u_2|^2$ correspond to the probabilities of getting the spin along $+Z$ and $-Z$ axes, respectively, and accordingly, they (u_1 and u_2) satisfy the relation $u_1^2 + u_2^2 = 1$.

Let us start with the general spin wave function,

$$\chi = \begin{pmatrix} u_1 \\ u_2 \end{pmatrix} = \begin{pmatrix} \cos\alpha \; e^{i\beta} \\ \sin\alpha \end{pmatrix} \tag{24}$$

Using this spin wave function, the expectation values of the Pauli spin matrices can be calculated those are in the form:

$$\begin{aligned} \langle\sigma_x\rangle &= \langle\chi|\sigma_x|\chi\rangle \\ &= \begin{pmatrix} \cos\alpha \; e^{-i\beta} & \sin\alpha \end{pmatrix} \begin{pmatrix} 0 & 1 \\ 1 & 0 \end{pmatrix} \begin{pmatrix} \cos\alpha \; e^{i\beta} \\ \sin\alpha \end{pmatrix} \\ &= \sin 2\alpha \cos\beta \end{aligned} \tag{25}$$

$$\begin{aligned} \langle\sigma_y\rangle &= \langle\chi|\sigma_y|\chi\rangle \\ &= \begin{pmatrix} \cos\alpha \; e^{-i\beta} & \sin\alpha \end{pmatrix} \begin{pmatrix} 0 & -i \\ i & 0 \end{pmatrix} \begin{pmatrix} \cos\alpha \; e^{i\beta} \\ \sin\alpha \end{pmatrix} \\ &= -\sin 2\alpha \sin\beta \end{aligned} \tag{26}$$

$$\begin{aligned} \langle\sigma_z\rangle &= \langle\chi|\sigma_z|\chi\rangle \\ &= \begin{pmatrix} \cos\alpha \; e^{-i\beta} & \sin\alpha \end{pmatrix} \begin{pmatrix} 1 & 0 \\ 0 & -1 \end{pmatrix} \begin{pmatrix} \cos\alpha \; e^{i\beta} \\ \sin\alpha \end{pmatrix} \\ &= \cos 2\alpha \end{aligned} \tag{27}$$

Therefore, the polarization vector $\vec{P}$ is,

$$\vec{P} \equiv \begin{pmatrix} P_x \\ P_y \\ P_z \end{pmatrix} = \begin{pmatrix} \sin 2\alpha \cos 2\beta \\ -\sin 2\alpha \sin\beta \\ \cos 2\alpha \end{pmatrix} \tag{28}$$

From the above matrix equality we get,

$$\begin{aligned} \sin 2\alpha \cos\beta &= P_x \\ -\sin 2\alpha \sin\beta &= P_y \\ \cos 2\alpha &= P_z \end{aligned} \tag{29}$$

The above three expressions in Eq. (29) can be solved to get the values,

$$\begin{aligned} \sin\alpha &= \sqrt{\frac{1-P_z}{2}} \\ \cos\alpha &= \sqrt{\frac{1+P_z}{2}} \\ \cos\beta &= \frac{P_x}{\sqrt{1-{P_z}^2}} \end{aligned} \tag{30}$$

With these expressions, the components u_1 and u_2 of the spin wave function can be written in terms of the polarization vector components as,

$$\begin{aligned} u_1 &= \sqrt{\frac{1+P_z}{2}} e^{i[\cos^{-1}(\frac{P_x}{\sqrt{1-{P_z}^2}})]} \\ u_2 &= \sqrt{\frac{1-P_z}{2}} \end{aligned} \tag{31}$$

Therefore, the probabilities of getting the up ($\uparrow$) and down ($\downarrow$) spins along $+Z$ and $-Z$ axes

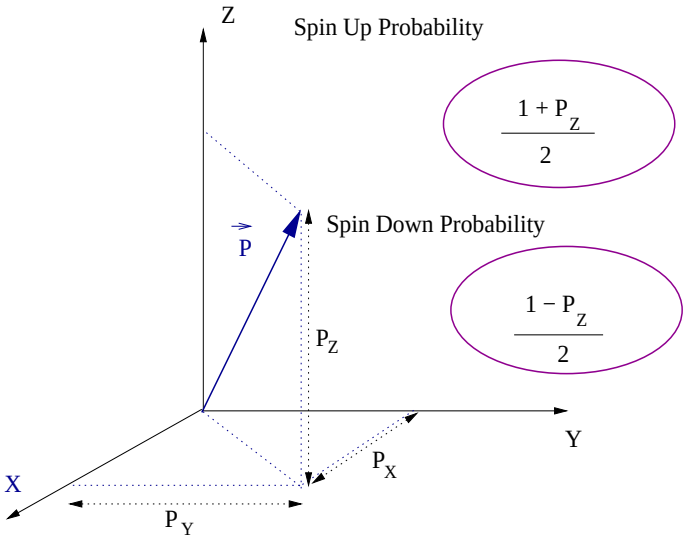

Figure 2: Coherent decomposition of a single spin along the quantization axis Z.

become,

$$\begin{aligned} |u_1|^2 &= \frac{1+P_z}{2} \\ |u_2|^2 &= \frac{1-P_z}{2} \end{aligned} \tag{32}$$

which obey the relation $|u_1|^2 + |u_2|^2 = 1$. The result is schematically described in Fig. 2.

3.3 Spin Polarized Electron Beam

In actual practice we generally deal with an ensemble of spin polarized electrons, instead of a single polarized electron, and accordingly, the formalism described above needs to be extended for the description of an ensemble. If all the individual electrons are aligned to a particular direction, the beam is said to be completely polarized, while for a partially polarized beam the individual electrons are aligned in different directions. So in short we can write,
$|\vec{P}| = 1$: pure spin state.
$0 < |\vec{P}| < 1$: mixed spin state.
For the complete description of a spin polarized electron beam, both the number of electrons and the spin polarization vector ($\vec{P}$) have to be specified. Here a basic question that arises is, how one can determine $\vec{P}$ for an ensemble of spin polarized electrons ?
Now each individual electron i (say), having its spin orientation along ξ axis can be completely described by a linear combination of two components $u_1^i \begin{pmatrix} 1 \\ 0 \end{pmatrix}$ and $u_2^i \begin{pmatrix} 0 \\ 1 \end{pmatrix}$ along ξ and $-\xi$ axes, respectively. Thus, for the entire electron beam, the probabilities of getting the up and down spin electrons along ξ are,

$$n_\uparrow = \sum_i |u_1^i|^2, \qquad n_\downarrow = \sum_i |u_2^i|^2 \tag{33}$$

The degree of spin polarization P_ξ of a spin polarized electron beam relative to a quantization axis ξ is defined as,

$$P_\xi = \frac{n_\uparrow - n_\downarrow}{n_\uparrow + n_\downarrow} \tag{34}$$

where, $\uparrow$ means along $+\xi$ axis and $\downarrow$ means along $-\xi$ axis. In terms of intensity of magnetization (I) the spin polarization can also be defined which is in the form,

$$P = \frac{I^{maj} - I^{min}}{I^{maj} + I^{min}} \tag{35}$$

The +ve value of $|\vec{P}|$ manifests that the polarization is along majority spin direction, while, the $-$ve value of $|\vec{P}|$ means the polarization is along minority spin direction.

3.4 An alternative formulation for the description of spin polarization

The polarization vector $\vec{P}$ can also be written in the density matrix formulation as,

$$\vec{P} \equiv \begin{pmatrix} P_x \\ P_y \\ P_z \end{pmatrix} = \begin{pmatrix} Tr(\sigma_x \rho) \\ Tr(\sigma_y \rho) \\ Tr(\sigma_z \rho) \end{pmatrix} \tag{36}$$

where, ρ is the polarization density matrix which can be expressed in the form,

$$\rho = \frac{1}{2}\begin{pmatrix} 1+P_z & P_x - iP_y \\ P_x + iP_y & 1-P_z \end{pmatrix} \tag{37}$$

3.5 Spin analyzer

Spin analyzer is a particular device that is used for the measurement of spin polarization of an electron beam. It consists of a spin filter and an electron detector. Only the intensities of 'spin up' and 'spin down' electrons relative to the quantization axis can be measured with the aid of a spin analyzer. It does not measure their phases. Generally three parameters are used to measure the properties of a spin analyzer. They are as follow.
(i) A direction of maximum transmission, denoted by the unit vector $\hat{e}$ in space.
(ii) A transmission factor T_R^{max} for electrons that are fully polarized along $\hat{e}$.
(iii) A transmission factor T_R^{min} for electrons that are fully polarized along $-\hat{e}$.
Now to reveal the polarization of incident electron beam with an analyzer, the response of the analyzer has to be known. The response is completely described by two factors, T_R and ΔT_R, where,

$$\begin{aligned} T_R &= \frac{1}{2}(T_R^{max} + T_R^{min}) \\ \Delta T_R &= \frac{1}{2}(T_R^{max} - T_R^{min}) \end{aligned} \tag{38}$$

Choosing the quantization direction as the maximum transmission direction, spin analyzer can be completely described by the transmission filter matrix as,

$$\begin{aligned} \hat{F} &= T_R \begin{pmatrix} 1+\frac{\Delta T_R}{2T_R} & 0 \\ 0 & 1-\frac{\Delta T_R}{2T_R} \end{pmatrix} \\ &= \begin{pmatrix} T_R + \frac{1}{2}\Delta T_R & 0 \\ 0 & T_R - \frac{1}{2}\Delta T_R \end{pmatrix} \end{aligned} \tag{39}$$

If T_R and ΔT_R are known parameters, the polarization of the incident beam along ξ axis can be measured by two successive experiments. Now the incident beam and the transmitted beam are related by the expression,

$$\frac{I}{I_0} = Tr(\hat{\rho_0}\hat{F}) \tag{40}$$

where,

$$\rho_0 = \frac{1}{2}\begin{pmatrix} 1+{P_\xi}^0 & {P_\eta}^0 - i{P_\zeta}^0 \\ {P_\eta}^0 + i{P_\zeta}^0 & 1-{P_\xi}^0 \end{pmatrix} \tag{41}$$

Therefore, we can write,

$$\begin{aligned} \frac{I}{I_0} &= T_R + \frac{1}{2}P_\xi^0 \Delta T_R \\ \Rightarrow P_\xi^0 &= \left[\frac{I}{I_0} - T_R\right]\frac{2}{\Delta T_R} \end{aligned} \tag{42}$$

3.6 Spin Filter

An electron beam becomes spin polarized after passing through a spin filter. The transmitted beam becomes polarized even if the incident beam is unpolarized.
Let the incident and transmitted beams are characterized by, $(I_0, \hat{\rho_0}, \vec{P^0})$ and $(I, \hat{\rho}, \vec{P})$.
Let us consider an incident unpolarized electron beam with $\vec{P^0} = 0$. So, $P_\xi^0 = P_\eta^0 = P_\zeta^0 = 0$. So the polarization density matrix becomes,

$$\hat{\rho_0} = \frac{1}{2}\begin{pmatrix} 1 & 0 \\ 0 & 1 \end{pmatrix} \tag{43}$$

So, we can write,

$$\frac{I}{I_0} = Tr(\hat{\rho_0}\hat{F}) = \frac{1}{2}Tr(\hat{F}) = T_R \tag{44}$$

Now, the polarization density matrix for the transmitted beam is defined by the relation,

$$\hat{\rho} = \frac{I_0}{I}\hat{\rho_0}\hat{F} = \frac{\hat{\rho_0}\hat{F}}{T_R} \tag{45}$$

So,

$$\hat{\rho} = \frac{1}{2}\begin{pmatrix} 1 + \frac{\Delta T_R}{2T_R} & 0 \\ 0 & 1 - \frac{\Delta T_R}{2T_R} \end{pmatrix} \tag{46}$$

Comparing Eqs. 41 and 46 we can write,
$P_\zeta = 0 = P_\eta$ and $P_\xi = \frac{\Delta T_R}{2T_R}$.
So the polarization matrix becomes,

$$\vec{P} \equiv \begin{pmatrix} P_\eta \\ P_\zeta \\ P_\xi \end{pmatrix} = \begin{pmatrix} 0 \\ 0 \\ \frac{\Delta T_R}{2T_R} \end{pmatrix} \neq 0 \tag{47}$$

Therefore, the incident unpolarized beam has got some polarization along the quantization direction after passing through the spin filter. T_R and ΔT_R can be calculated by determining T_{max} and T_{min} where they can be evaluated through experiment, by the same way that is used to calibrate 'Mott polarization detector'.

3.7 Fundamental interactions of a spin polarized electron beam with matter

Experimental observation suggests that when a spin polarized electron beam traverses through a nonmagnetic noble metal, like Cu, the polarization of the beam becomes reduced, while the spin polarization gets increased when the spin polarized electron beam traverses through a ferromagnetic metal. It is generally suggested that these changes are due to 'spin flips', i.e., transition from up spin state to down spin state and vice versa. In actual practice, the change in spin polarization is not typically due to spin flips, but there are some other processes which are responsible for this mechanism. For illustrative purposes here we mention some of them as follow.

• Spin precession: It is associated with a phase shift between the up and down spin wave functions which provides a precession of $\vec{P}$ about the quantization axis, keeping the magnitude ($|\vec{P}|$) as invariant.
• Spin exchange scattering: This is related to the transition from one spin channel to the other spin channel. The polarization vector $\vec{P}$ rotates relative to the quantization axis ξ, with a change in the component P_ξ.
• Spin dephasing: It is related to the out of phase precession of the individual spins about the quantization axis, and accordingly, the magnitude of the component $P_\perp$ (perpendicular to the quantization direction) gets decreased. In non-magnetic materials, this effect may lead to complete spin randomization.
• Spin selective absorption: This particular phenomenon originates from the preferential scattering of spin in one spin channel. It causes a rotation of $\vec{P}$ relative to the quantization axis resulting a change in magnitude, i.e., $|\vec{P}| \neq |\vec{P^0}|$, where $|\vec{P^0}|$ is the initial amplitude of the polarization vector.

3.8 Two Current Model

The total number of electrons in each atom those are responsible for electrical conduction, $n(E_F)$, is directly proportional to the density of states at E_F. This proposes that Cu to be a bad conductor, while, Fe, Co and Ni having a large value of $n(E_F)$ to be good conductors. But in actual practice, Cu has the highest conductivity among all of these transition metals. Naturally, a question arises why there is such a discrepancy ?

This discrepancy was removed by Neville Mott. He guessed that 's' electrons carry electric current, and, due to scattering of electrons from 's' band to 'd' band, the electrical resistance appears. Therefore, stronger scattering takes place when more 'd' states are available. Since this scattering is 'spin selective', only the electrons having the same spin can jump from 's' band to 'd' band. Spin mixing between the two channels are forbidden.

In the 'two current model', the high resistivity of the transition metals with a partially filled 'd' shell is thus produced by scattering of 's' electrons to the empty 'd' states. The modern band theory supports the strong hybridization of 's' and 'd' electrons, and accordingly, the excitations

from ‘s’ to ‘d’ states arise naturally.

In the ‘two current model’, the two spin states carry the electric current separately and independently of each other. This is due to the spin selective scattering process of ‘s’ electrons to the vacant ‘d’ band, which is the key aspect of this model. The basic feature of the ‘two current model’ is based on ‘Fermi’s Golden rule’ which states that the scattering probability of the conduction electrons, that leads to an increase in resistivity, is proportional to the density of the vacant ‘d’ states available above the Fermi energy.

Since the conduction in two different spin channels occurs independently, the net conductivity becomes,

$$\sigma = \sigma_{\uparrow} + \sigma_{\downarrow} \tag{48}$$

where, $\sigma_{\uparrow} = \frac{n_{\uparrow} e^2 \tau_{\uparrow}}{m_e}$ and $\sigma_{\downarrow} = \frac{n_{\downarrow} e^2 \tau_{\downarrow}}{m_e}$. This ‘two current model’ is valid in diffusive as well as in

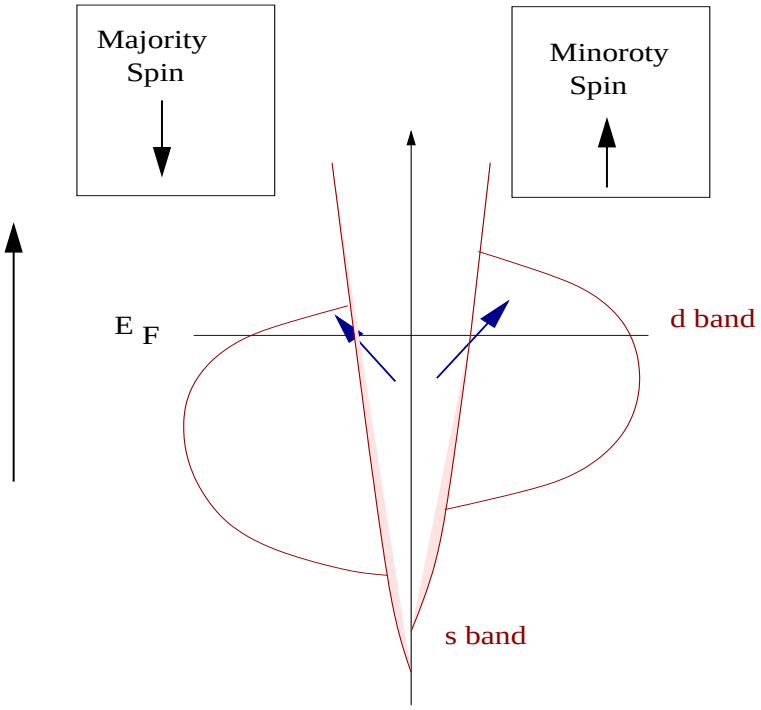

Figure 3: Spin excitations in the two current model.

ballistic regime.

So, in a nutshell what we can say about ‘two current model’ is:

The two current model predicts that, electric current flows in two separate spin channels independently, and the total conductivity is obtained by adding the individual contributions of the two separate spin channels. The resistivity gets increased when the electrons in one of the spin channels undergo spin conserving scattering from ‘s’ band to the empty states of ‘d’ band.

The 'two current model' is illustrated schematically in Fig. 3.

4 Formal theory of spin transport

4.1 Spin accumulation voltage

Let us consider a steady current is flowing along the direction x through the interface between a ferromagnetic metal (FM) and a non-magnetic metal (NM). The quantitative description of this current can be formulated in terms of 'spin dependent chemical potential'.

The 'spin dependent chemical potential' of majority electrons of the system is specified by the energy change which is associated with the addition of one majority electron to the system.

If no current flows through the interface, Fermi levels of both the metals (FM and NM) will be rearranged to the identical value μ_0, where,

$$\mu_0 = \frac{\mu_\uparrow + \mu_\downarrow}{2} \tag{49}$$

According to Ohm's law, when a current flows from FM to NM along x direction, we can write,

$$\frac{\partial \mu_0}{\partial x} = -\frac{e}{\sigma} j \tag{50}$$

where, e is the electronic charge and σ is the total electrical conductivity due to up and down spin electrons, i.e., $\sigma = \sigma_\uparrow + \sigma_\downarrow$. Spin flips, required to make transitions from one conductivity channel to the other, can be neglected at low temperatures. But, this is a good approximation even at room temperature, since the spin flip length is larger than the electronic mean free path at that temperature.

Now interesting spin dependent phenomena must occur at the interface between a ferromagnetic metal, characterized by a preferential conduction in one spin channel, and a non-magnetic metal having equal conduction for both the spin channels. From the charge neutrality condition at the interface, we get, j = constant. Therefore, in μ-x curve, μ_0 becomes a straight line with a change in slope at the interface, as $\sigma_N \neq \sigma_F$, where σ_N and σ_F correspond to the conductivities of the non-magnetic and ferromagnetic metals, respectively. But the description is not complete because of the fact that, in the ferromagnetic metal unequal number of up and down spin electrons provides different electrical conductivities associated with each spin channel.
Let us define,

$$\begin{aligned} \sigma_F^\uparrow &= \alpha_F \sigma_F \\ \sigma_F^\downarrow &= (1-\alpha_F)\sigma_F \end{aligned} \tag{51}$$

where, α_F is a parameter lying between 0 to 1. Now, due to the asymmetry of conduction in the two spin channels, $\alpha_F \neq 0.5$. In a bulk ferromagnet, minority spin channel has the lower conductivity, and therefore, $\alpha_F > 0.5$.
Asymmetry in conduction through the two spin channels results asymmetric current. Now we define,

$$\begin{aligned} {j_F}^{\uparrow} &= \beta_F j \\ {j_F}^{\downarrow} &= (1-\beta_F) j \end{aligned} \tag{52}$$

and,

$$\begin{aligned} {j_N}^{\uparrow} &= \beta_N j \\ {j_N}^{\downarrow} &= (1-\beta_N) j \end{aligned} \tag{53}$$

where, β_F and β_N are the two parameters. The spin polarization $\vec{P}$ of the current is defined as,

$$\begin{aligned} P &= \frac{j^{\uparrow} - j^{\downarrow}}{j^{\uparrow} + j^{\downarrow}} \\ &= 2\beta_\alpha - 1 \end{aligned} \tag{54}$$

where, α corresponds to $F(N)$ when the spin polarization is defined in case of FM(NM). When the spin polarized current enters from FM ($\beta_F \neq 0.5$) to NM ($\beta_N = 0.5$), $\beta_N \neq 0.5$ and $P \neq 0$ at

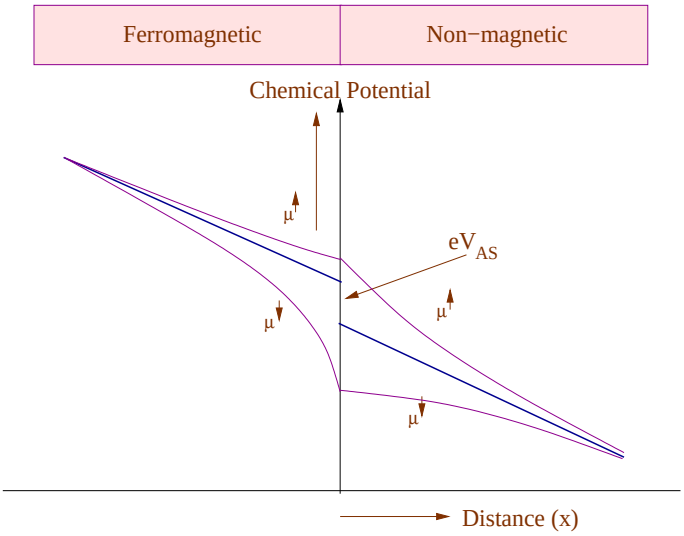

Figure 4: Variation of spin dependent chemical potentials across the interface, when a steady current is flowing from a ferromagnetic metal to a non-magnetic metal.

the interface. This is due to the fact that, spin flips are rare, so it will take time to equilibrate to the value $\beta_N = 0.5$ away from the interface. This introduces a voltage drop at the interface, the

so-called 'spin accumulation voltage' (V_{AS}) as shown in Figs. 4 and 5. The chemical potentials due to up ($\uparrow$) and down ($\downarrow$) spins, $\mu^{\uparrow}$ and $\mu^{\downarrow}$, must be continuous across the interface. For a non-magnetic metal since the two spin channels conduct equally, μ_0 will be the average of $\mu^{\uparrow}$ and $\mu^{\downarrow}$. On the other hand, it is a weighted average for a ferromagnetic metal. Thus, for non-magnetic metals (NM),

$$\mu_{0N} = \frac{1}{2}(\mu^{\uparrow} + \mu^{\downarrow}) \tag{55}$$

and for ferromagnetic metals (FM),

$$\mu_{0F} = \alpha_F \mu^{\uparrow} + (1 - \alpha_F)\mu^{\downarrow} \tag{56}$$

When current flows from FM to NM, V_{AS} can be written as,

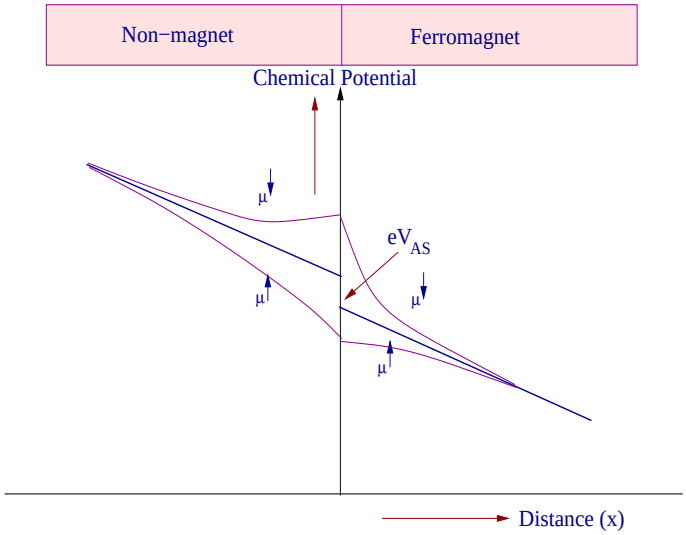

Figure 5: Variation of spin dependent chemical potentials across the interface, when a steady current is flowing from a non-magnetic metal to a ferromagnetic metal.

$$\begin{aligned} eV_{AS} &= \mu_{0F}(x=0) - \mu_{0N}(x=0) \\ &= \left[\alpha_F - \frac{1}{2}\right](\mu^{\uparrow}(0) - \mu^{\downarrow}(0)) \end{aligned} \tag{57}$$

In this particular case, $\alpha_F > 0.5$. Thus, $V_{AS} \neq 0$ and $\mu^{\uparrow}(0) > \mu^{\downarrow}(0)$. For the reverse situation, i.e., when the current flows from NM to FM, we can write,

$$\begin{aligned} eV_{AS} &= \mu_{0N}(x=0) - \mu_{0F}(x=0) \\ &= \left[\alpha_F - \frac{1}{2}\right](\mu^{\downarrow}(0) - \mu^{\uparrow}(0)) \end{aligned} \tag{58}$$

Hence, in this situation, $\mu^{\downarrow}(0) > \mu^{\uparrow}(0)$.

To summarize, the spin accumulation voltage (V_{AS}) can be defined as the jump in spin averaged chemical potentials, developed at the FM/NM interface, because of the asymmetric conduction of the two spin channels through the interface.

4.2 Diffusion equation for spins

A spin voltage is defined as the difference between spin up and down chemical potentials and it reflects the difference in the number of electrons in the two current carrying spin channels. The diffusion equation for the up ($\uparrow$) and down ($\downarrow$) spins can be written in terms of their chemical potentials as,

$$D\frac{d^2(\mu^\uparrow - \mu^\downarrow)}{dx^2} = \frac{\mu^\uparrow - \mu^\downarrow}{\tau_{se}} \tag{59}$$

Solving Eq. 59 we get,

$$\mu^\uparrow - \mu^\downarrow = [\mu^\uparrow(0) - \mu^\downarrow(0)]e^{-\frac{x}{\Lambda}} \tag{60}$$

where, Λ is given by, $\Lambda = \sqrt{D\tau_{se}}$. The decrease of spin voltage ($\mu^\uparrow - \mu^\downarrow$) with distance from the interface is determined by the characteristic equilibrium distance Λ, the so-called 'spin diffusion length'. Thus the spin dependent chemical potentials ($\mu^\uparrow$ and $\mu^\downarrow$) equilibrate away from the interface ($x = 0$) over a characteristic length (Λ) and a characteristic time (τ_{se}). In order to observe the spin dependent transport through a conductor, the sample size should be less than or comparable to the 'spin diffusion length'.

5 Spin transport at atomic scale

5.1 Introduction

Recent progress in nanoscience and nanotechnology has enabled us to develop various magnetic materials and magneto devices which reveal several fascinating phenomena. This new era in the study of magnetism has been initiated in 1988 after the discovery of Giant Magneto Resistance (GMR) effect [2] observed in magnetic multilayers formed by alternating magnetic and non-magnetic materials.

In the absence of an external magnetic field, the exchange coupling between adjacent magnetic layers through the non-magnetic one aligns the magnetization vector anti-parallel to each other. Then, when a magnetic field, strong enough to overcome the anti-ferromagnetic coupling is applied, all the magnetization vectors align along the field direction. This new parallel configuration exhibits an electrical resistance which is much smaller than that of the anti-ferromagnetic configuration. This drastic change in resistance is known as the GMR effect which is illustrated in Fig. 6. Mathematical definition of GMR is given by,

$$R = \frac{R_{AP} - R_P}{R_P} \tag{61}$$

In normal GMR effect, $R_{AP} > R_P$, and R is unbounded. Another definition used for GMR is,

$$R' = \frac{R_{AP} - R_P}{R_{AP}} \tag{62}$$

In this particular case, $0 \leq R' \leq 1$.

Inverse GMR effect has also been found in some materials for which $R_P > R_{AP}$. The study of GMR effect is of fundamental importance as it established the fact that the spin of an electron can also take an important role in transport phenomena. Today, the study of GMR effect has drawn much attention from academic circuit to commercial levels [3] as GMR based magnetic data storage devices are used in every computers. Not only that, spintronics in low dimensional systems provides some real advantages over bulk metals and semiconductors. In molecular systems, the conventional mechanisms for spin decoherence (spin orbit coupling, scattering from

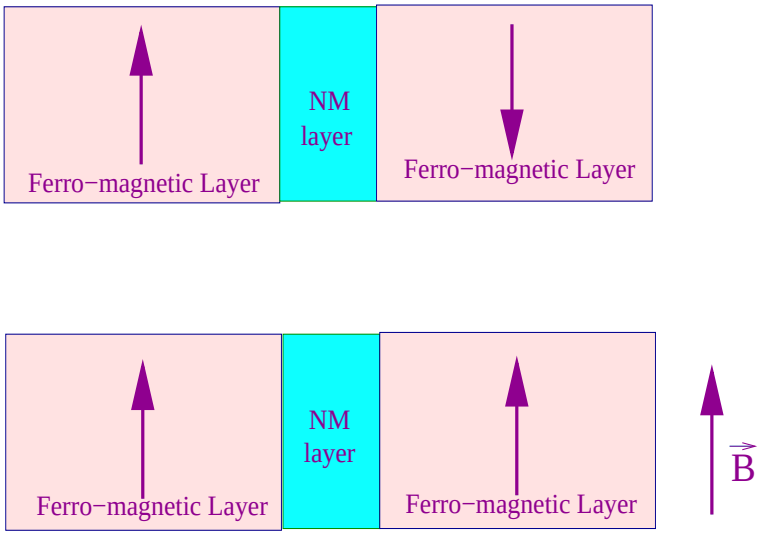

Figure 6: Schematic representation of GMR sensor.

paramagnetic impurities, etc.) get reduced. Hence, in nanoscale systems, we can expect the spin coherence time to be several orders of magnitude larger than in bulk systems. Therefore, the study of spin dependent transport and spin dynamics is of great importance to understand and to develop the field, spintronics.

Spin dependent transport through mesoscopic systems has attracted rich attention in the development of spintronics [4, 5, 6, 7]. Several experimental efforts have been made to study spin transport in quantum dots (QD) [8, 9, 10, 11] and molecular systems [11, 12, 13, 14].

In these systems, electrical resistance depends on the spin state of electrons passing through the device, and it can be controlled by an applied magnetic field. This is due to the imbalance in transmission probability for spin up and down electrons through the device [15, 16].

The spin dependent transport through nanostructures such as a QD system, can be investigated by coupling it to magnetic or nonmagnetic leads and passing a current through the

system [14, 17, 18, 19, 20]. Several theoretical as well as experimental studies have been made on the spin transport through quantum dot devices [21, 22, 23].

Aim of the model that has been analyzed below is to study analytically the coherent spin dependent transport of a magnetic QD system attached to nonmagnetic leads, with the magnetic quantum dot (MQD) device having an arbitrary magnetic configuration. This analysis has been done using Transfer matrix method in the framework of tight-binding Hamiltonian [24, 25, 26, 27, 28].

5.2 Description of the model and formalism

The model chosen is a heterostructure formed by a sequence of magnetic and nonmagnetic sites connected to nonmagnetic leads. The spin dependent electronic transport through this structure has been studied including the spin flip scattering effect. The heterostructure is basically a repetition of a chosen unit cell formed by magnetic and nonmagnetic atoms. The geometry of the NM/MQD/NM structure is shown schematically in Figs. 7 and 8. The direction of

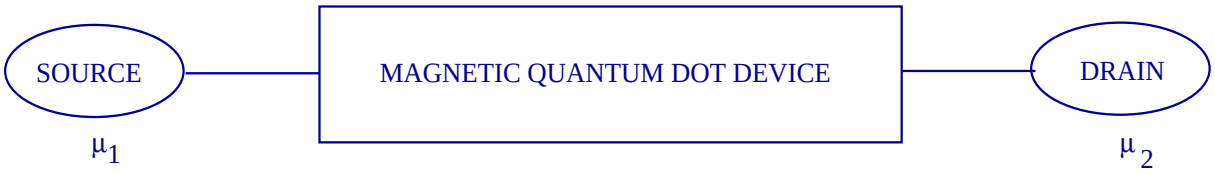

Figure 7: A magnetic quantum dot device (magnetic spacer) is attached to source and drain.

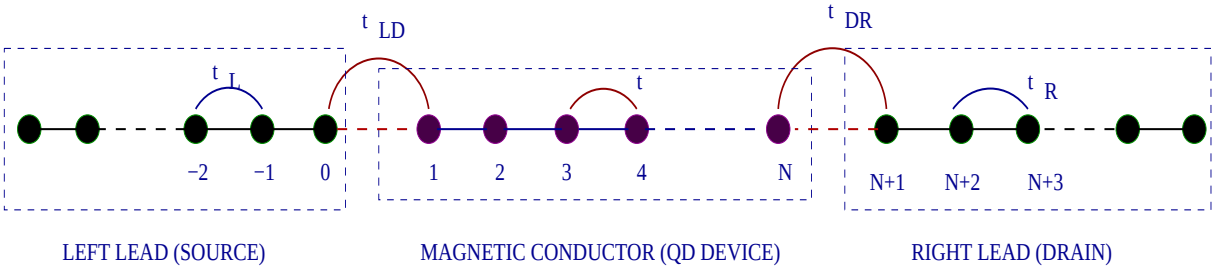

Figure 8: Schematic view of the model. A magnetic conductor is connected to nonmagnetic source and drain.

magnetization on each magnetic site in the MQD device is chosen to be arbitrary, specified in each site n, which in spherical polar coordinate system is defined by two angles θ_n and ϕ_n. Here θ_n is the angle between magnetization direction and the Z axis, ϕ_n is the azimuthal angle of magnetization measured from X axis at site n as shown in Fig. 9. The whole system can be described by a Hamiltonian of the general form,

$$H = H_L + H_{LD} + H_D + H_{DR} + H_R \tag{63}$$

The spin polarized electrons for a N-site quantum dot can be described within the effective one-electron approximation in tight-binding framework and the nearest-neighbor approximation as,

$$H_D = \sum_n \mathbf{c_n^\dagger} \left(\epsilon_\mathbf{n} - \vec{\mathbf{h}_\mathbf{n}}.\vec{\sigma}\right) \mathbf{c_n} + \sum_\mathbf{n} \left(\mathbf{c_n^\dagger t_{n,n+1} c_{n+1}} + \mathbf{c_{n+1}^\dagger t_{n,n+1} c_n}\right) \tag{64}$$

where, $\mathbf{c_n^\dagger} = \begin{pmatrix} c_{n\uparrow}^\dagger & c_{n\downarrow}^\dagger \end{pmatrix}$,

$\mathbf{c_n} = \begin{pmatrix} c_{n\uparrow} \\ c_{n\downarrow} \end{pmatrix}$,

$\epsilon_\mathbf{n} = \begin{pmatrix} \epsilon_{n\uparrow} & 0 \\ 0 & \epsilon_{n\downarrow} \end{pmatrix}$,

$\mathbf{t_{n,n+1}} = \begin{pmatrix} t_{n,n+1} & 0 \\ 0 & t_{n,n+1} \end{pmatrix}$

The term ϵ_n of Eq. 64 describes the on-site energy. The term $\vec{h_n}.\vec{\sigma}$ describes the interaction of electrons with the magnetic atoms in MQD device. This term allows the spin flips at the magnetic sites. h_n is the amplitude of the spin flip parameter at site n. σ is the Pauli spin

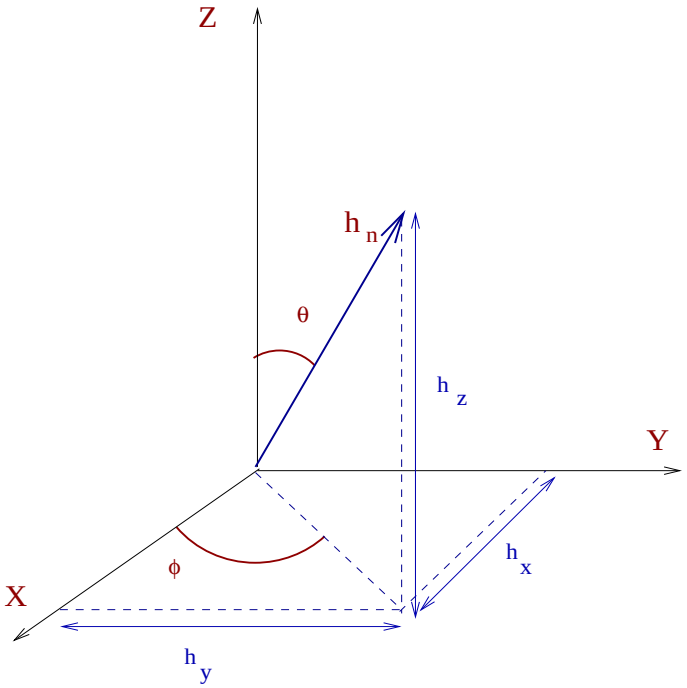

Figure 9: Decomposition of h_n in spherical polar coordinates.

operator having components $(\sigma_x, \sigma_y, \sigma_z)$. Spin flip scattering is dependent on the magnetic moment orientation of the atoms in MQD device with respect to the Z axis. The term $t_{n,n+1}$ is the nearest-neighbor hopping integral, ${c^\dagger}_{n\sigma}(c_{n\sigma})$ is the creation(annihilation) operator for an

electron on site n with spin σ. The Hamiltonian of the left(right) lead is defined as,

$$H_{L(R)} = \sum_i \mathbf{c_i^\dagger \epsilon_i c_i} + \sum_i \left(\mathbf{c_i^\dagger t_{L(R)} c_{i+1}} + \mathbf{c_{i+1}^\dagger t_{L(R)} c_i} \right) \tag{65}$$

where $t_{L(R)}$ refers to the hopping integral between the sites of the left(right) lead. Finally, the Hamiltonian that corresponds to the coupling of the MQD device to the leads can be expressed in the form,

$$H_{LD(RD)} = \left(\mathbf{c_{0(N+1)}^\dagger t_{LD(RD)} c_{1(N)}} + \mathbf{c_{1(N)}^\dagger t_{LD(RD)} c_{0(N+1)}} \right) \tag{66}$$

Throughout this study, it has been assumed that the nonmagnetic leads are ideal, i.e., their resistances have been neglected. The main contribution to the resistance in this ballistic device has come from contact resistance and spin scattering in MQD.
Using this model the spin dependent transmission coefficients are calculated to investigate the transport properties, in transfer matrix formalism. In this calculation the Schrödinger equation is written in terms of $\psi_{n,\sigma}$ (localized Wannier basis), which express the amplitude of the wave function at site n, with energy E and spin σ.

5.2.1 Transfer Matrix method

In order to calculate the spin dependent transmission probabilities, the Schrödinger equation for the electron wave function must be solved in the MQD device. So the starting point is the time independent Schrödinger equation in the MQD device, which can be written as,

$$H|\phi\rangle = E|\phi\rangle \tag{67}$$

where,

$$|\phi\rangle = \sum_i [\psi_{i\uparrow}|i\uparrow\rangle + \psi_{i\downarrow}|i\downarrow\rangle] \tag{68}$$

Here, $|\phi\rangle$ is written as a linear combination of spin up and spin down Wannier states. Now,

$$\begin{aligned} \vec{h}.\vec{\sigma} &= h_x\sigma_x + h_y\sigma_y + h_z\sigma_z \\ &= \begin{pmatrix} h\cos\theta_n & h\sin\theta_n e^{-i\phi_n} \\ h\sin\theta_n e^{i\phi_n} & -h\cos\theta_n \end{pmatrix} \end{aligned} \tag{69}$$

So the Hamiltonian H_D for the whole MQD device can be written as,

$$\begin{aligned} H_D &= \sum_n \left(c_{n\uparrow}^\dagger c_{n\downarrow}^\dagger \right) \begin{pmatrix} \epsilon_{n\uparrow} - h\cos\theta_n & -h\sin\theta_n e^{-i\phi_n} \\ -h\sin\theta_n e^{i\phi_n} & \epsilon_{n\downarrow} + h\cos\theta_n \end{pmatrix} \begin{pmatrix} c_{n\uparrow} \\ c_{n\downarrow} \end{pmatrix} + \\ &\quad \sum_n \left[\left(c^\dagger{}_{n\uparrow} c^\dagger{}_{n\downarrow} \right) \begin{pmatrix} t & 0 \\ 0 & t \end{pmatrix} \begin{pmatrix} c_{n+1,\uparrow} \\ c_{n+1,\downarrow} \end{pmatrix} + \left(c^\dagger{}_{n+1,\uparrow} c^\dagger{}_{n+1,\downarrow} \right) \begin{pmatrix} t & 0 \\ 0 & t \end{pmatrix} \begin{pmatrix} c_{n,\uparrow} \\ c_{n,\downarrow} \end{pmatrix} \right] \\ &= H_1 + H_2 \end{aligned} \tag{70}$$

where,

$$\begin{aligned} H_1 &= \sum_n |n\uparrow\rangle\left(\epsilon_{n\uparrow} - h\cos\theta_n\right)\langle n\uparrow| - \sum_n |n\uparrow\rangle h\sin\theta_n e^{-i\phi_n}\langle n\downarrow| - \\ &\quad \sum_n |n\downarrow\rangle h\sin\theta_n e^{i\phi_n}\langle n\uparrow| + \sum_n |n\downarrow\rangle\left(\epsilon_{n\downarrow} + h\cos\theta_n\right)\langle n\downarrow| \qquad (71) \\ H_2 &= \sum_n |n\uparrow\rangle t\langle n+1,\uparrow| + \sum_n |n\downarrow\rangle t\langle n+1,\downarrow| + \\ &\quad \sum_n |n+1,\uparrow\rangle t\langle n\uparrow| + \sum_n |n+1,\downarrow\rangle t\langle n\downarrow| \qquad (72) \end{aligned}$$

Operating H on $|\phi\rangle$ we get the following two equations relating the Wannier amplitudes on site n of the MQD device with the neighboring $n \pm 1$ sites,

$$\left(E - \epsilon_n + h_n\cos\theta_n\right)\psi_{n\uparrow} + h_n\sin\theta_n e^{-i\phi_n}\psi_{n\downarrow} = t\psi_{n+1,\uparrow} + t\psi_{n-1,\uparrow} \qquad (73)$$

$$h_n\sin\theta_n e^{i\phi_n}\psi_{n\uparrow} + \left(E - \epsilon_n - h_n\cos\theta_n\right)\psi_{n\downarrow} = t\psi_{n+1,\downarrow} + t\psi_{n-1,\downarrow} \qquad (74)$$

Transfer matrix for the nth site relates the wave amplitudes of nth site with that of $(n-1)$th and $(n+1)$th sites. So we can write the transfer matrix equation for the nth site as,

$$\begin{pmatrix} \psi_{n+1\uparrow} \\ \psi_{n+1\downarrow} \\ \psi_{n\uparrow} \\ \psi_{n\downarrow} \end{pmatrix} = \begin{pmatrix} \frac{E-\epsilon_n+h_n cos\theta_n}{t} & \frac{h_n sin\theta_n e^{-i\phi_n}}{t} & -1 & 0 \\ \frac{h_n sin\theta_n e^{i\phi_n}}{t} & \frac{E-\epsilon_n-h_n cos\theta_n}{t} & 0 & -1 \\ 1 & 0 & 0 & 0 \\ 0 & 1 & 0 & 0 \end{pmatrix} \begin{pmatrix} \psi_{n\uparrow} \\ \psi_{n\downarrow} \\ \psi_{n-1\uparrow} \\ \psi_{n-1\downarrow} \end{pmatrix} \qquad (75)$$

So the total transfer matrix for the whole MQD device can be written as, $P = \prod_{l=N}^{1} P_l$ where,

$$P_n = \begin{pmatrix} \frac{E-\epsilon_n+h_n cos\theta_n}{t} & \frac{h_n sin\theta_n e^{-i\phi_n}}{t} & -1 & 0 \\ \frac{h_n sin\theta_n e^{i\phi_n}}{t} & \frac{E-\epsilon_n-h_n cos\theta_n}{t} & 0 & -1 \\ 1 & 0 & 0 & 0 \\ 0 & 1 & 0 & 0 \end{pmatrix} \qquad (76)$$

For the whole lead-MQD-lead system, the transfer matrix (T) that relates the wave amplitude from the left lead ((-1)th and 0th sites) to the right lead ($(N+1)$th and $(N+2)$th sites) is given by,

$$\begin{pmatrix} \psi_{N+2\uparrow} \\ \psi_{N+2\downarrow} \\ \psi_{N+1\uparrow} \\ \psi_{N+1\downarrow} \end{pmatrix} = T \begin{pmatrix} \psi_{0\uparrow} \\ \psi_{0\downarrow} \\ \psi_{-1\uparrow} \\ \psi_{-1\downarrow} \end{pmatrix} \qquad (77)$$

where,

$$T = M_R.P.M_L \qquad (78)$$

Here, M_R = the transfer matrix for right boundary, i.e., $(N+1)$th site. It relates the wave amplitudes from Nth site (in the MQD device) to $(N+1)$th site (in the right lead). Similarly, M_L = the transfer matrix for left boundary, i.e., 0th site. It relates the wave amplitudes from 1st site (in the MQD device) to (-1)th site (in the left lead).

5.2.2 To calculate M_L and M_R

Let us calculate M_L first. For the left (or right) lead, $\vec{h}.\vec{\sigma} = 0$. So the Hamiltonian for the lead (left or right) can be simplified as, $H_{\text{lead}} = H_1 + H_2$, where,

$$H_1 = \sum_n \left(|n\uparrow\rangle \epsilon_{n\uparrow} \langle n\uparrow| + |n\downarrow\rangle \epsilon_{n\downarrow} \langle\downarrow|\right) \tag{79}$$

and

$$H_2 = \sum_n \left(|n\uparrow\rangle t \langle n+1,\uparrow| + |n\downarrow\rangle t \langle n+1,\downarrow| + |n+1,\uparrow\rangle t \langle n\uparrow| + |n+1,\downarrow\rangle t \langle n\downarrow|\right) \tag{80}$$

We set $\epsilon_n = \epsilon_0$ for all n in the leads. Now, from the time independent Schrödinger equation, operating H on $|\phi\rangle$ we get two equations for 0th site, relating the wave amplitudes of 1st and -1th sites, as given below.

$$\begin{aligned} (E-\epsilon_0)\,\psi_{0\uparrow} &= t_{LD}\psi_{1\uparrow} + t_L\psi_{-1\uparrow} \\ (E-\epsilon_0)\,\psi_{0\downarrow} &= t_{LD}\psi_{1\downarrow} + t_L\psi_{-1\downarrow} \end{aligned} \tag{81}$$

Now in the lead, according to the tight-binding model,

$$\psi_n = Ae^{ikna} \tag{82}$$

So ψ_{-1} can be written in terms of ψ_0 as,

$$\psi_{-1} = \psi_0 e^{-i\beta_L} \tag{83}$$

where, $\beta_L = ka$ and

$$E = \epsilon_0 + 2t_{L(R)} cos\beta_{L(R)} \tag{84}$$

From Eqs. 81 and 82, ψ_1 can be expressed in terms of ψ_0 as,

$$\psi_1 = \left(\frac{t_L}{t_{LD}} e^{i\beta_L}\right)\psi_0 \tag{85}$$

Hence, the transfer matrix matrix equation for the 0th site is of the form,

$$\begin{pmatrix} \psi_{1\uparrow} \\ \psi_{1\downarrow} \\ \psi_{0\uparrow} \\ \psi_{0\downarrow} \end{pmatrix} = \begin{pmatrix} \frac{t_L}{t_{LD}}e^{i\beta_L} & 0 & 0 & 0 \\ 0 & \frac{t_L}{t_{LD}}e^{i\beta_L} & 0 & 0 \\ 0 & 0 & e^{i\beta_L} & 0 \\ 0 & 0 & 0 & e^{i\beta_L} \end{pmatrix} \begin{pmatrix} \psi_{0\uparrow} \\ \psi_{0\downarrow} \\ \psi_{-1\uparrow} \\ \psi_{-1\downarrow} \end{pmatrix} \tag{86}$$

Similarly, from the time independent Schrödinger equation, operating H on $|\phi\rangle$ we get two equations for $(N+1)$th site, relating the wave amplitudes of Nth and $(N+2)$th sites as given below.

$$\begin{aligned} (E-\epsilon_0)\psi_{N+1\uparrow} &= t_R\psi_{N+2\uparrow} + t_{DR}\psi_{N-1\uparrow} \\ (E-\epsilon_0)\psi_{N+1\downarrow} &= t_R\psi_{N+2\downarrow} + t_{DR}\psi_{N-1\downarrow} \end{aligned} \tag{87}$$

Exactly as before the transfer matrix matrix equation for the $(N+1)$th site can be written as,

$$\begin{pmatrix} \psi_{N+2\uparrow} \\ \psi_{N+2\downarrow} \\ \psi_{N+1\uparrow} \\ \psi_{N+1\downarrow} \end{pmatrix} = \begin{pmatrix} e^{i\beta_R} & 0 & 0 & 0 \\ 0 & e^{i\beta_R} & 0 & 0 \\ 0 & 0 & \frac{t_{DR}}{t_R}e^{i\beta_L} & 0 \\ 0 & 0 & 0 & \frac{t_{DR}}{t_R}e^{i\beta_L} \end{pmatrix} \begin{pmatrix} \psi_{N+1\uparrow} \\ \psi_{N+1\downarrow} \\ \psi_{N\uparrow} \\ \psi_{N\downarrow} \end{pmatrix} \tag{88}$$

Therefore,

$$\begin{aligned} M_L &= \text{the transfer matrix for the left boundary} \\ &= \begin{pmatrix} \frac{t_L}{t_{LD}}e^{i\beta_L} & 0 & 0 & 0 \\ 0 & \frac{t_L}{t_{LD}}e^{i\beta_L} & 0 & 0 \\ 0 & 0 & e^{i\beta_L} & 0 \\ 0 & 0 & 0 & e^{i\beta_L} \end{pmatrix} \end{aligned} \tag{89}$$

$$\begin{aligned} M_R &= \text{the transfer matrix for the right boundary} \\ &= \begin{pmatrix} e^{i\beta_R} & 0 & 0 & 0 \\ 0 & e^{i\beta_R} & 0 & 0 \\ 0 & 0 & \frac{t_{DR}}{t_R}e^{i\beta_L} & 0 \\ 0 & 0 & 0 & \frac{t_{DR}}{t_R}e^{i\beta_L} \end{pmatrix} \end{aligned} \tag{90}$$

5.2.3 To calculate the transmission probability of up and down spin electrons

Thus the transfer matrix for the whole system (lead-MQD-lead) can be written as,

$$\begin{aligned} T &= \text{matrix for (N+1)th site.product matrix for N-th site to 1st site. matrix for 0-th site} \\ &= M_R.P.M_L \end{aligned} \tag{91}$$

In order to calculate the transmission coefficient for the incident electrons with up or down spin using the transfer matrix method, the wave function amplitudes (Wannier amplitudes) have to be specified on proper atomic sites.

Case 1: Up spin incidence in the left lead.

The eigenvalue equation involving the transfer matrix relating the Wannier amplitudes from sites $(N+2)$ and $(N+1)$ to sites 0 and -1 is given by Eq. 77.
Let,
$\rho^{\uparrow\uparrow}$ = Reflection amplitude for up spin ($\uparrow$) reflected as up spin ($\uparrow$).
$\rho^{\uparrow\downarrow}$ = Reflection amplitude for up spin ($\uparrow$) reflected as down spin ($\downarrow$).
$\tau^{\uparrow\uparrow}$ = Transmission amplitude for up spin ($\uparrow$) transmitted as up spin ($\uparrow$).
$\tau^{\uparrow\downarrow}$ = Transmission amplitude for up spin ($\uparrow$) transmitted as down spin ($\downarrow$).
Now, for the left lead, the wave amplitudes at the sites 0 and -1 can be written as,

$$\begin{aligned}
\psi_{-1\uparrow} &= e^{-i\beta_L} + \rho^{\uparrow\uparrow} e^{i\beta_L} \\
\psi_{-1\downarrow} &= \rho^{\uparrow\downarrow} e^{i\beta_L} \\
\psi_{0\uparrow} &= 1 + \rho^{\uparrow\uparrow} \\
\psi_{0\downarrow} &= \rho^{\uparrow\downarrow}
\end{aligned} \tag{92}$$

Similarly, for the right lead, the wave amplitudes at the sites $(N+1)$ and $(N+2)$ become,

$$\begin{aligned}
\psi_{N+2\uparrow} &= \tau^{\uparrow\uparrow} e^{i(N+2)\beta_R} \\
\psi_{N+2\downarrow} &= \tau^{\uparrow\downarrow} e^{i(N+2)\beta_R} \\
\psi_{N+1\uparrow} &= \tau^{\uparrow\uparrow} e^{i(N+1)\beta_R} \\
\psi_{N+1\downarrow} &= \tau^{\uparrow\downarrow} e^{i(N+1)\beta_R}
\end{aligned} \tag{93}$$

Therefore, the transfer matrix eigenvalue equation can be rewritten in terms of these wave function amplitudes as,

$$\begin{pmatrix} \tau^{\uparrow\uparrow} e^{i(N+2)\beta_R} \\ \tau^{\uparrow\downarrow} e^{i(N+2)\beta_R} \\ \tau^{\uparrow\uparrow} e^{i(N+1)\beta_R} \\ \tau^{\uparrow\downarrow} e^{i(N+1)\beta_R} \end{pmatrix} = T. \begin{pmatrix} 1 + \rho^{\uparrow\uparrow} \\ \rho^{\uparrow\downarrow} \\ e^{-i\beta_L} + \rho^{\uparrow\uparrow} e^{i\beta_L} \\ \rho^{\uparrow\downarrow} e^{i\beta_L} \end{pmatrix} \tag{94}$$

Solving the above equation we can get the values of $\tau^{\uparrow\uparrow}$ and $\tau^{\uparrow\downarrow}$. The transmission coefficients $T^{\uparrow\uparrow}$ and $T^{\uparrow\downarrow}$ are defined as the ratio of the transmitted flux to the incident flux as,

$$T_{\uparrow\uparrow} = \frac{t_R \sin\beta_R}{t_L \sin\beta_L} |\tau^{\uparrow\uparrow}|^2$$

$$T_{\uparrow\downarrow} = \frac{t_R \sin\beta_R}{t_L \sin\beta_L}|\tau^{\uparrow\downarrow}|^2 \tag{95}$$

Therefore, the total transmission probability for spin up is,

$$T_\uparrow = T_{\uparrow\uparrow} + T_{\uparrow\downarrow} \tag{96}$$

Case 2: Down spin incidence in the left lead.

Similarly, for a down spin incidence in the left lead, the amplitudes at sites -1, 0, $(N+1)$ and $(N+2)$ are given by,

$$\begin{aligned}
\psi_{0\uparrow} &= \rho^{\downarrow\uparrow} \\
\psi_{0\downarrow} &= 1 + \rho^{\downarrow\downarrow} \\
\psi_{-1\uparrow} &= \rho^{\downarrow\uparrow} e^{i\beta_L} \\
\psi_{-1\downarrow} &= e^{-i\beta_L} + \rho^{\downarrow\downarrow} e^{i\beta_L}
\end{aligned} \tag{97}$$

and

$$\begin{aligned}
\psi_{N+2\uparrow} &= \tau^{\downarrow\uparrow} e^{i(N+2)\beta_R} \\
\psi_{N+2\downarrow} &= \tau^{\downarrow\downarrow} e^{i(N+2)\beta_R} \\
\psi_{N+1\uparrow} &= \tau^{\downarrow\uparrow} e^{i(N+1)\beta_R} \\
\psi_{N+1\downarrow} &= \tau^{\downarrow\downarrow} e^{i(N+1)beta_R}
\end{aligned} \tag{98}$$

So, as before, the transfer matrix equation for down spin incidence can be rewritten in terms of these wave amplitudes as,

$$\begin{pmatrix} \tau^{\downarrow\uparrow} e^{i(N+2)\beta_R} \\ \tau^{\downarrow\downarrow} e^{i(N+2)\beta_R} \\ \tau^{\downarrow\uparrow} e^{i(N+1)\beta_R} \\ \tau^{\downarrow\downarrow} e^{i(N+1)\beta_R} \end{pmatrix} = T. \begin{pmatrix} \rho^{\downarrow\uparrow} \\ 1 + \rho^{\downarrow\downarrow} \\ \rho^{\downarrow\uparrow} e^{i\beta_L} \\ e^{-i\beta_L} + \rho^{\downarrow\downarrow} e^{i\beta_L} \end{pmatrix} \tag{99}$$

This equation can be solved to compute $\tau^{\downarrow\downarrow}$ and $\tau^{\downarrow\uparrow}$.
The transmission coefficients $T^{\downarrow\downarrow}$ and $T^{\downarrow\uparrow}$ are defined by the ratio of the transmitted flux to the incident flux as,

$$\begin{aligned}
T_{\downarrow\downarrow} &= \frac{t_R \sin\beta_R}{t_L \sin\beta_L}|\tau^{\downarrow\downarrow}|^2 \\
T_{\downarrow\uparrow} &= \frac{t_R \sin\beta_R}{t_L \sin\beta_L}|\tau^{\downarrow\uparrow}|^2
\end{aligned} \tag{100}$$

Therefore, the total transmission probability for spin down is,

$$T_{\downarrow} = T_{\downarrow\downarrow} + T_{\downarrow\uparrow} \tag{101}$$

At low temperatures, the transport of such mesoscopic systems is ballistic and coherent. In this regime, transmitted spin dependent current flowing through the interacting region with arbitrary magnetic configurations, symmetrically attached to the two NM leads is given by the relation [29, 30],

$$I_{\sigma\sigma'}(V) = \frac{e}{\pi\hbar} \int_{-\infty}^{+\infty} (f_S - f_D)\, T_{\sigma\sigma'}(E)\; dE \tag{102}$$

where, $f_{S(D)} = f\left(E - \mu_{S(D)}\right)$ gives the Fermi distribution function with the electrochemical potential $\mu_{S(D)} = E_F \pm eV/2$. Thus, $I_{\sigma\sigma'}$ is calculated by determining $T_{\sigma\sigma'}$ from Eqs. 95 and 100.

5.3 Numerical results and discussion

In order to investigate the spin transport properties through the MQD device in NM/MQD/NM heterostructures, we perform some numerical calculations. To do this we assume that the MQD device consists of several unit cells (see Figs. 10, 13, 16 and 19) that are made up of some magnetic (A) and nonmagnetic (B) atoms having different magnetic moment orientation. By applying an external magnetic field, the magnetization direction of the NM/MQD/NM system can be switched.

To illustrate the results, let us first mention the values of the different parameters those are considered throughout our numerical calculations. For simplicity, all the on-site energies both in the two leads and in MQD device are taken to be zero. The nearest-neighbor hopping integral t in the MQD device is set to 1, and, in the two side attached leads the hopping strength $t_{L(R)}$ is also fixed at 1. The Fermi energy E_F is fixed at 0. The spin flip parameter is chosen as $h = 0.5$. To narrate the coupling effect [31, 32, 33, 34], throughout the study we focus our results for the two limiting cases depending on the strength of the coupling of the MQD device to the source and drain. Case $\mathcal{A}$: The weak-coupling limit. It is described by the condition $\tau_{L(R)} << t$. For this regime we choose $\tau_L = \tau_R = 0.2$. Case B: The strong-coupling limit. This is specified by the condition $\tau_{L(R)} \sim t$. In this particular regime, we set the values of the parameters as $\tau_L = \tau_R = 0.8$. For the sake of simplicity we choose the unit $c = e = h = 1$.

Case 1:

Let us start with a periodic MQD system in the parallel magnetic configuration. The MQD device is made up of several unit cells, where each unit cell contains four magnetic (A) atoms, each having parallel magnetic moment orientation. The schematic view of the unit cell configuration is given in Fig. 10. Here we study the variation of the conductance g as a function of the injecting

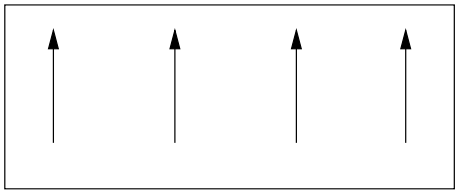

Figure 10: Unit cell configuration 1 made up of four magnetic atoms A, each having parallel magnetic moment.

electron energy E, both for the weak- and strong-coupling limits, respectively. The results are focused for the two separate cases, respectively. One is the transmission of up spin ($\uparrow$) as up spin ($\uparrow$) and the other is the transmission of up spin ($\uparrow$) as down spin ($\downarrow$), i.e., the case of spin flip. The nature of the conductance spectra for a typical MQD device with total number of site $N = 64$ in the limit of weak-coupling is shown in Fig. 11. Figure 11(a) predicts the conductance due to the transmission of up spin as up spin. On the other hand, the conductance involving only the spin flip effect, i.e., transmission of up spin as down spin, is given in Fig. 11(b). From Fig. 11(a) it is observed that, for some particular energies the conductance exhibits fine resonant

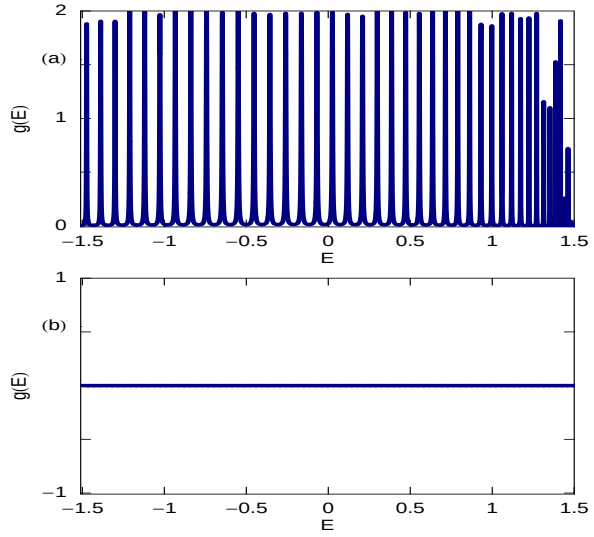

Figure 11: g-E spectra for a MQD device with the unit cell configuration 1, in the weak-coupling limit. (a) $g_{\uparrow\uparrow}$ and (b) $g_{\uparrow\downarrow}$.

peaks, while the conductance drops to zero for other energies. At the resonant energies where the conductance approaches the value 2, the transmission probability T goes to unity, since the relation $g = 2T$ follows from the Landauer conductance formula, $g = 2(e^2/h)T$, with $e = h = 1$. All these resonant peaks are associated with the energy eigenvalues of the MQD device, and accordingly, we can say that the conductance spectrum manifests itself the electronic structure of the MQD device. Now, Fig. 11(b) shows zero transmission probability for transmission of up spin as down spin, for this type of unit cell configuration. The effect of coupling is quite interest-

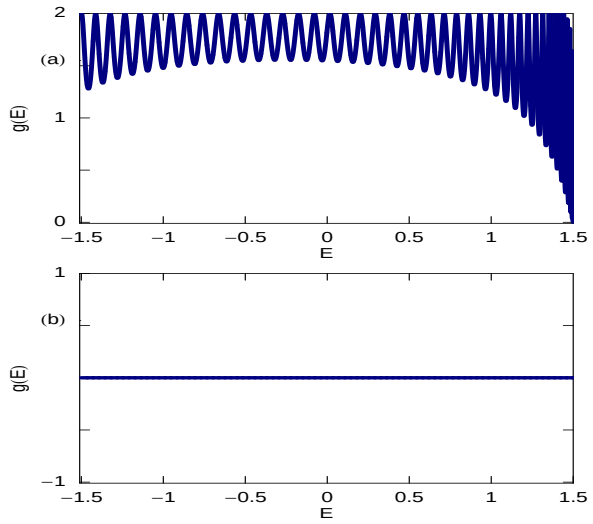

Figure 12: g-E spectra for a MQD device with the unit cell configuration 1, in the strong-coupling limit. (a) $g_{\uparrow\uparrow}$ and (b) $g_{\uparrow\downarrow}$.

ing. For our illustrative purposes, in Fig. 12 we plot the g-E spectra for the same MQD device ($N = 64$) in the limit of strong-coupling, where (a) and (b) correspond to the same meaning as in Fig. 11. Figure 12(a) predicts that, all these resonant peaks get substantial widths compared to the weak-coupling limit. The contribution for the broadening of the resonant peaks appears from the broadening of the energy levels of the MQD device in this strong-coupling limit [35]. Hence by tuning the coupling strength, we can get the electron transmission across the MQD device for the wider range of energies and it provides an important signature in the study of current-voltage (I-V) characteristics. Similar to the weak-coupling limit, for this strong-coupling case also, there is no spin flipping, and accordingly, we get zero transmission probability for the transmission of up spin as down spin.

Case 2:

Now we focus on the conductance behavior for a periodic MQD system having anti-parallel magnetic moment orientation. The MQD device is made up of several unit cells, where each unit cell contains four magnetic (A) atoms, arranged antiferromagnetically. The schematic view of the unit cell configuration is illustrated in Fig 13. For representative examples, in Fig. 14

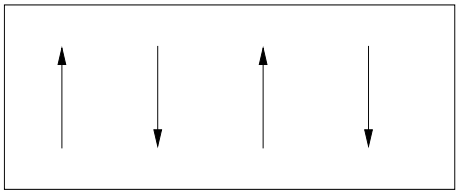

Figure 13: Unit cell configuration 2 made up of four magnetic atoms A, having anti-parallel magnetic moment.

we plot the conductance-energy spectra for a typical MQD device considering $N = 64$, in the

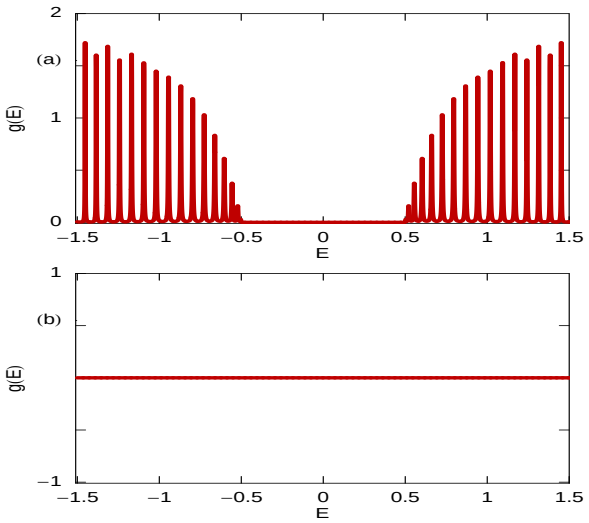

Figure 14: g-E spectra for a MQD device with the unit cell configuration 2, in the weak-coupling limit. (a) $g_{\uparrow\uparrow}$ and (b) $g_{\uparrow\downarrow}$.

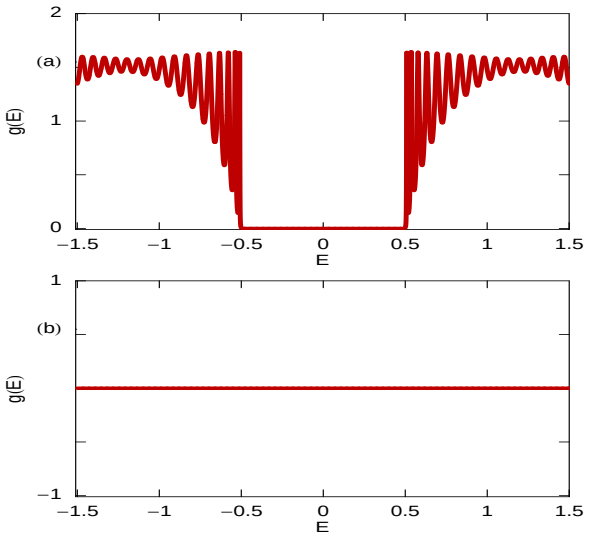

Figure 15: g-E spectra for a MQD device with the unit cell configuration 2, in the strong-coupling limit. (a) $g_{\uparrow\uparrow}$ and (b) $g_{\uparrow\downarrow}$.

limit of weak-coupling, where (a) and (b) represent the identical meaning as in Fig. 11. Similar to the above case, here we also see that for some particular energies the non-zero value of the transmission probability of up spin as up spin is achieved. While, the transmission probability of up spin as down spin becomes exactly zero for the entire energy range (Fig. 14(b)), since there is no spin flip effect in this cell configuration. On the other hand, with the increase of the MQD-lead coupling strength, all the resonant peaks get broadened. The results for the

strong-coupling limit are shown in Fig. 15, where (a) and (b) represent the identical meaning as above. From both these spectra (Fig. 14(a) and Fig. 15(a)), we get additional one feature, which is the appearance of a global energy gap in the conductance spectrum. The gap appears symmetrically about the energy $E = 0$ with width $2h$ (since $h_n = h$ for all the sites). This reveals that the electron conduction takes place beyond the energy h, and no electron conduction takes place when the energy $E < h$. Thus by controlling the strength of h, we can tune the electron conduction. This behavior can be much more clearly explained from our study of current-voltage characteristics which we will describe in the forthcoming section.

Case 3:

Next, we concentrate our study on the behavior of electron conduction for a periodic MQD device which is made up of several unit cells, where each unit cell contains four magnetic (A)

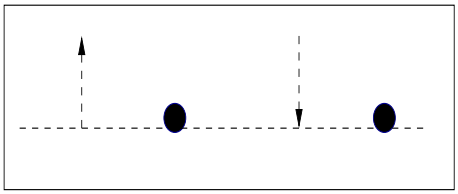

Figure 16: Unit cell configuration 3 made up of four magnetic and nonmagnetic atoms A and B, A having antiparallel magnetic moment.

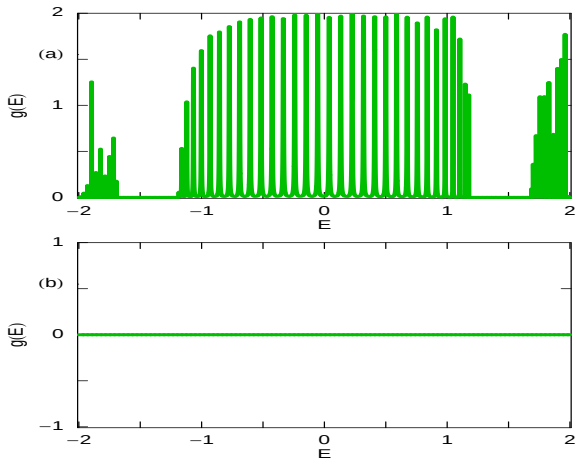

Figure 17: g-E spectra for a MQD device with the unit cell configuration 3, in the weak-coupling limit. (a) $g_{\uparrow\uparrow}$ and (b) $g_{\uparrow\downarrow}$.

and nonmagnetic (B) atoms, arranged alternately. The unit cell configuration is schematically given in Fig. 16. The variation of the conductance g with the energy E for a typical MQD device with $N = 64$ in the limit of weak-coupling is shown in Fig. 17. While, the results for the strong-coupling case are plotted in Fig. 18. For both these two cases, (a) and (b) correspond to the identical meaning as described earlier. The properties of the resonant peaks both for the two

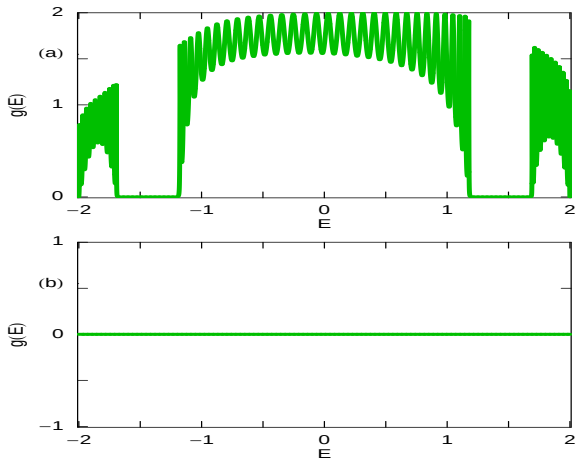

Figure 18: g-E spectra for a MQD device with the unit cell configuration 3, in the strong-coupling limit. (a) $g_{\uparrow\uparrow}$ and (b) $g_{\uparrow\downarrow}$.

coupling cases, i.e., sharp peaks in the weak-coupling limit and broadened peaks in the limit of strong-coupling, remain unchanged like the previous unit cell configurations. Also, the behavior of getting up spin as down spin through this MQD device remains invariant as before. The argument of this vanishing transmission probability is exactly similar as we mentioned earlier. For this particular cell configuration we get additional one interesting feature which is related to the existence of the global energy gaps at the two distinct regions of the energy E (see Fig. 17(a) and Fig. 18(a)). The widths of these two gaps are exactly identical to each other, which is given by h. The existence of a global energy gap manifests that the system acts as an insulator along the perpendicular direction in the long length of MQD device. Here we get two such global energy gaps, and accordingly, this particular MQD device can be identified as double gap spin valve system, that can be used as a mutual spin switch.

Case 4:

Finally, we consider the particular case where each magnetic moment is oriented at an angle θ_n with respect to the vertical Z direction. For convenience, we consider a single unit cell which contains six magnetic moments. The unit cell configuration is schematically presented in Fig. 19. For illustrative examples, in Fig. 20 we plot the conductance-energy spectra for a MQD device

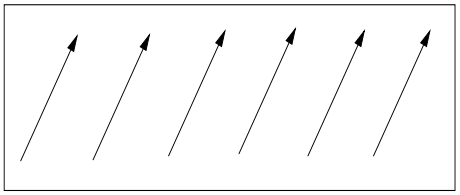

Figure 19: Unit cell configuration 4 made up of six magnetic atoms with their magnetic moments oriented at an angle θ with respect to the Z axis.

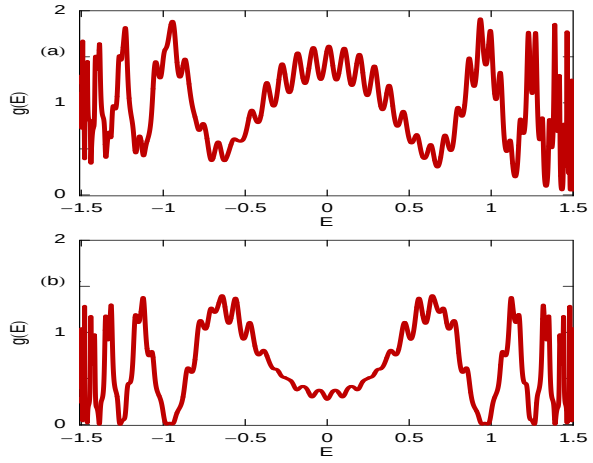

Figure 20: g-E spectra for a MQD device with the unit cell configuration 4, in the strong-coupling limit. (a) $g_{\uparrow\uparrow}$ and (b) $g_{\uparrow\downarrow}$. θ is chosen as $\pi/3$.

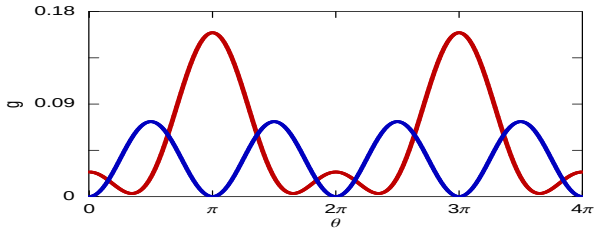

Figure 21: $g_{\uparrow\uparrow}$-θ (red curve) and $g_{\uparrow\downarrow}$-θ (blue curve) for a MQD device with the unit cell configuration 4, in the weak-coupling limit. The energy E is fixed at 0.25.

considering $N = 64$ in the limit of strong-coupling. Figure 20(a) represents the g-E spectrum associated with the transmission of up spin as up spin, while Fig. 20(b) corresponds to the g-E curve associated with the spin flip effect, i.e., the transmission of up spin as down spin. For this unit cell configuration, we assume that all the magnetic moments are aligned at an angle $\theta = \pi/3$ ($\theta_n = \theta$ for all n) with respect to the preferred Z direction. Quite interestingly we see that, the MQD device with this particular unit cell configuration exhibits spin flip transmission. The reason for non-zero spin flip transmission probability is as follow. The interaction of spin of the injected electron with the local magnetic moments associated with each site of the MQD device is given by the term $\vec{h_n}.\vec{\sigma}$ in the Hamiltonian (Eq. 64). Unlike for unit cell configurations 1, 2 and 3, where the moments are taken to be either parallel or anti-parallel to Z axis, in this case all the local moments are aligned at an angle θ with respect to Z axis, i.e., they have non-vanishing x and y components. Therefore, the interaction term contains σ_x and σ_y and so also σ_+ and σ_-, which are responsible for spin flip. Now, to incorporate the dependence of θ on conductance, in Fig. 21 we present the results for a MQD device considering $N = 10$, where the red curve corresponds to the conductance ($g_{\uparrow\uparrow}$) due to pure spin transmission and the blue curve represents the conductance ($g_{\uparrow\downarrow}$) due to spin flip transmission.

5.3.1 Current-Voltage characteristics

All the basic features of spin dependent transmission become much more clearly visible from our study of current-voltage (I-V) characteristics. The current through the MQD device can be computed by integrating the transmission function T, as prescribed in Eq. 102. The transmission function varies exactly similar to that of the conductance spectrum, differ only in magnitude by the factor 2 since the relation $g = 2T$ holds from the Landauer conductance formula. Here we describe the I-V characteristics for all these four different unit cell configurations one by one.

Case 1:

First, we describe the results for the unit cell configuration 1. As illustrative examples, in Fig. 22 we show the variation of the current (I) as a function of the applied bias voltage (V) for a typical MQD device with $N = 8$, where the first and second rows correspond to the results for the weak- and strong-coupling limits, respectively. In the limit of weak-coupling, current shows step-like

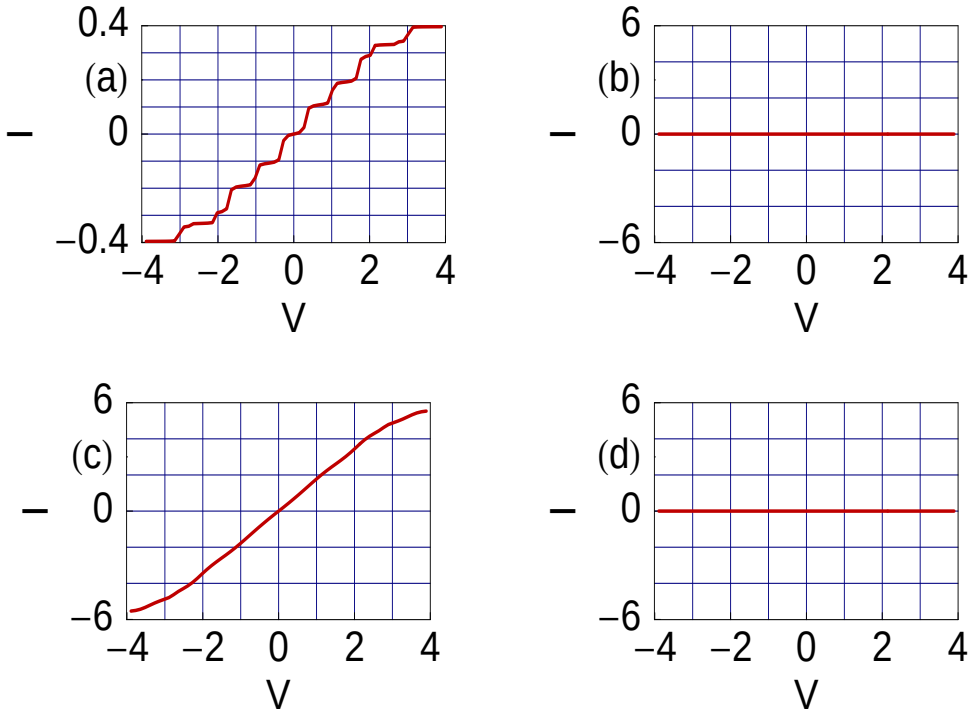

Figure 22: I-V curves for a MQD device with the unit cell configuration 1. The 1st and 2nd rows correspond to the weak- and strong-coupling limits, respectively. (a) $I_{\uparrow\uparrow}$, (b) $I_{\uparrow\downarrow}$, (c) $I_{\uparrow\uparrow}$ and (d) $I_{\uparrow\downarrow}$.

behavior as a function of bias voltage (see Fig. 22(a)). This is due to the presence of sharp resonant peaks in the conductance spectrum (Fig. 11(a)), as the current is obtained from the integration procedure of the function T. With the increase of the bias voltage, the difference in the electrochemical potentials of the leads increases, allowing more energy states accessible to

the injected electron to get passed through the MQD device from the source to drain. Therefore, the current increases providing a jump in the I-V characteristics. On the other hand, the current varies almost continuously when the coupling strength is increased (Fig. 22(c)), because in this coupling-limit the conductance peaks get broadened which provides larger current amplitude. Both in these two coupling limits, the current drops to zero for the entire bias voltage due to spin flip transmission.

Case 2:

Now we consider the case for the unit cell configuration 2. The I-V spectra for the MQD device

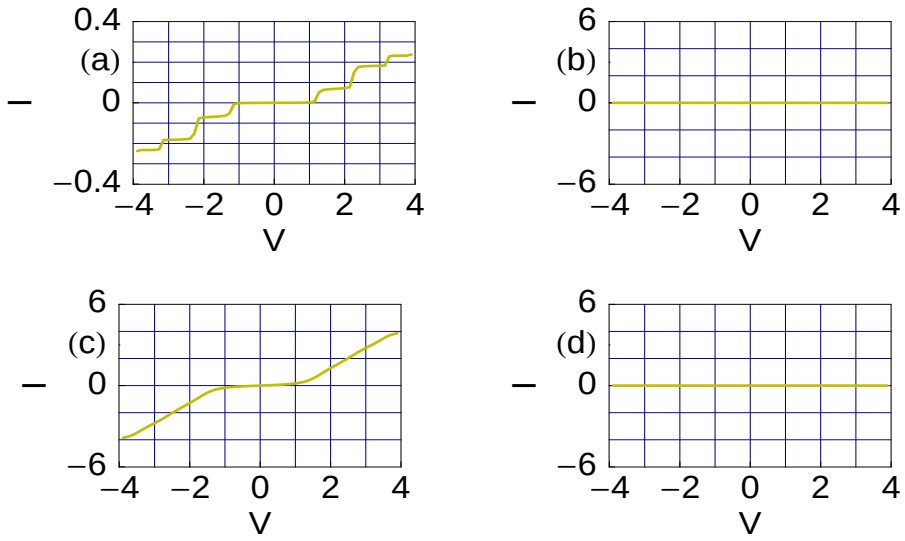

Figure 23: I-V curves for a MQD device with the unit cell configuration 2. The 1st and 2nd rows correspond to the weak- and strong-coupling limits, respectively. (a) $I_{\uparrow\uparrow}$, (b) $I_{\uparrow\downarrow}$, (c) $I_{\uparrow\uparrow}$ and (d) $I_{\uparrow\downarrow}$.

($N = 8$) are shown in Fig. 23, where the upper and lower rows correspond to the identical meaning as in Fig. 22. All the basic features due to the coupling are the same as discussed in previous case. But there is one additional important feature due to this type of unit cell configuration. Because of the presence of an energy gap in the conductance spectrum, the non-zero value of current is obtained after overcoming a threshold bias voltage.

Case 3:

Here we study the results for the unit cell configuration 3. The characteristic features of the I-V spectra for a MQD device with $N = 8$ is illustrated in Fig. 24. All the essential properties are almost invariant as presented in Fig. 22. In this particular cell configuration, the presence of the double energy gap in the conductance spectrum ensures the saturation like behavior in the current-voltage curve.

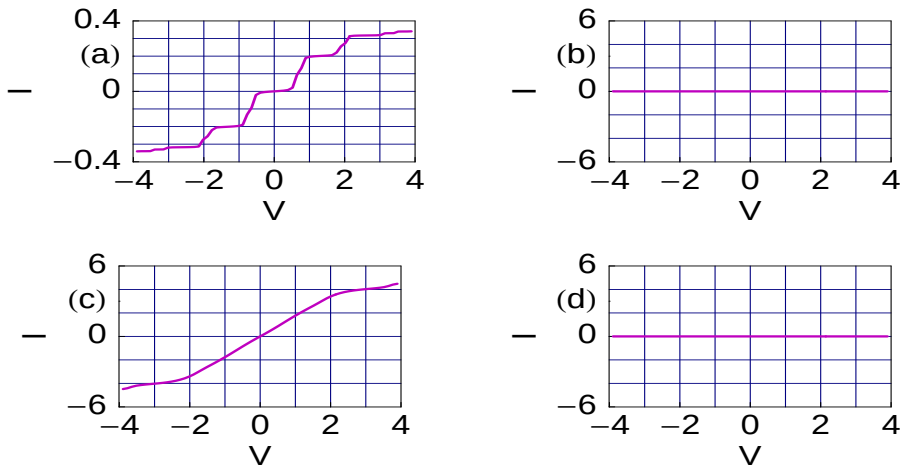

Figure 24: I-V curves for a MQD device with the unit cell configuration 3. The 1st and 2nd rows correspond to the weak- and strong-coupling limits, respectively. (a) $I_{\uparrow\uparrow}$, (b) $I_{\uparrow\downarrow}$, (c) $I_{\uparrow\uparrow}$ and (d) $I_{\uparrow\downarrow}$.

Case 4:

Finally, we come to the case where the unit cell of the MQD device is of the type configuration

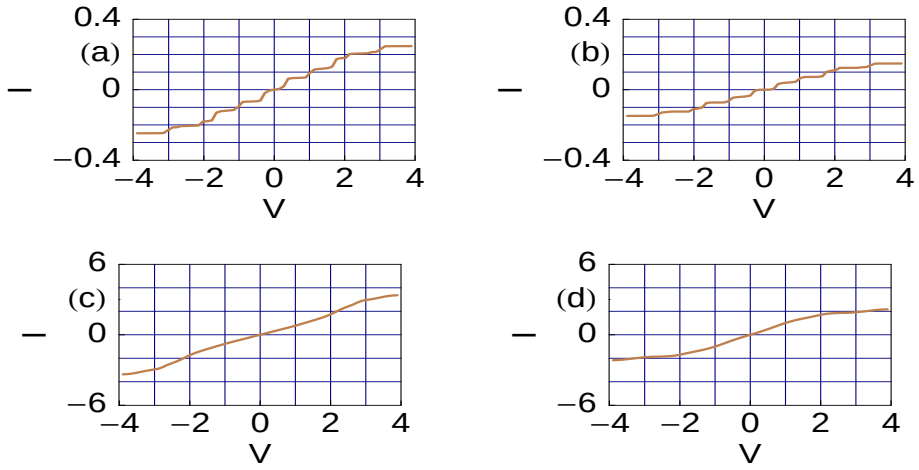

Figure 25: I-V curves for a MQD device with the unit cell configuration 4. Here we set $\theta = \pi/3$. The 1st and 2nd rows correspond to the weak- and strong-coupling limits, respectively. (a) $I_{\uparrow\uparrow}$, (b) $I_{\uparrow\downarrow}$, (c) $I_{\uparrow\uparrow}$ and (d) $I_{\uparrow\downarrow}$.

4. The results are shown in Fig. 25 for a MQD device considering $N = 8$. The new feature associated with the I-V characteristics in this case is the non-zero value of current due to spin flip transmission. Another important feature is that the magnitude of current due to spin flip transmission is much smaller than that of pure spin transmission.

6 Concluding remarks

In this dissertation, we have addressed some issues of spin polarized transport through matter. After introducing the new field-Spintronics, in the first section we have discussed about the generation of spin polarized electron source and its detailed mechanism. Then we have introduced the formal theory needed to study the spin polarized transport. Then we have talked about the 'Two Current Model' which is the stepping stone towards the development of modern spintronics. This model illustrates the fact that the two spin states of electrons conduct current separately and independently to each other, giving rise to different resistivities associated with each spin channel.

Next, we have tried to analyze the spin dependent transport in nanoscale systems. We have discussed spin transport in different types of NM/MQD/NM heterostructures, including the spin flip effect, within the tight-binding formulation.

The MQD spacer has been considered to be made up of an array of quantum dots, which is basically a repetition of unit cells chosen differently in different cases. For the first three cases the unit cells consist of magnetic QDs only, whereas in the last case it was thought to be periodically juxtaposed magnetic and nonmagnetic QDs.

In the theoretical formulation we have obtained the general formulae for calculating the spin dependent transmission coefficients, which depends on the arbitrary magnetic configuration of the MQD device.

Depending on the local magnetic moment orientation on each site, in the MQD device we obtained gapless, single-gap, double-gap conductance spectra, respectively, for both spin channels. In these cases the system acts as an insulator in a particular energy region, i.e., it can act as a mutual spin switch. We have got conductance spectra as a function of energy of injected electrons both in weak- and strong-coupling limits. The sharp resonant peaks appear in the conductance spectrum in the weak-coupling limit, whereas in the strong-coupling limit, due to the broadening of energy levels, except for the presence of global gap, conductance does not show zero value. We have also presented the variation of conductance with the angle made by the local magnetic moment with the quantization direction, both including and excluding spin flip effect.

Then, we have noticed the steplike behavior of I-V characteristics in the weak-coupling limit, which is a manifestation of quantized conductance of these kind of nanoscale systems. On the other hand, in the strong-coupling limit, the I-V spectra show almost continuous variation, instead of the step-like behavior.

Throughout this presentation, we have made several important assumptions. Here we discuss briefly about these approximations.

• All the calculations have been performed at 0K, but the results will not significantly change in non-zero finite temperature region also, as long as the thermal energy (k_BT) is less than the average spacing energy levels of the magnetic conductor.

• Secondly we have neglected the electron-electron correlation effect. The inclusion of electron-electron correlation is a major challenge to us, since over the last few years a lot of efforts have been made to incorporate this effect, but no proper theory has yet been developed.

• Electron-phonon interaction has also been neglected in our theoretical formulation, as we are dealing with 0K temperature. But even at non-zero finite temperature also we could neglect this effect. Because the broadening of energy levels due to electron-phonon interaction is much smaller than that of due to coupling of the MQD device with source and drain.

• The potential drops are considered at the boundaries only, not throughout the device.

• All the results have been presented for ordered systems, but in presence of impurity the transport properties can change that we have not been studied yet.

All the predicted results given above may be applied in designing spin polarized transistors in future.

References

[1] J. Stöhr and H. C. Siegmann, *Magnetism-From fundamentals to Nanoscale Dynamics*, Springer (2006).

[2] S. Maekawa and T. Shinjo, *Spin Dependent Transport in Magnetic Nanostructures*, CRC PRESS (2002).

[3] S. Sanvito, *Ab-initio Methods for Spin Transport at Nanoscale level*, Review Article (unpublished).

[4] G. Prinz, Phys. Today **48** (1995) 58.

[5] G. Prinz, Science **282** (1998) 1660.

[6] S. A. Wolf, D. D. Awschalom, R. A. Buhrman, J. M. Daughton, S. von Molnár, M. L. Roukes, A. Y. Chtchekanova, D. M. Treger, Science **294** (2001) 1488.

[7] M. Ziese and M. J. Thornton, *Spin Electronics*, Springer, Berlin (2001).

[8] M. Stopa, J. P. Bird, K. Ishibashi, Y. Aoyagi, T. Sugano, Phys. Rev. Lett. **76** (1996) 2145.

[9] R. López and D. Sánchez, Phys. Rev. Lett. **90** (2003) 116602.

[10] Z. H. Xiong, D. Wu, Z.V. Vardeny, J. Shi, Nature **427** (2004) 821.

[11] B. R. Bulka and S. Lipinski, Phys. Rev. B **67** (2003) 024404.

[12] M. Zwolak and M. D. Ventra, Appl. Phys. Lett. **81** (2002) 925.

[13] W. I. Babiaczyk and B. R. Bulka, J. Phys.: Condens. Matter **16** (2004) 4001.

[14] R. Pati, L. Senapati, P. M. Ajayan, S. K. Nayak, Phys. Rev. B **68** (2003) 100407.

[15] A. A. Shokri and A. Saffarzadeh, J. Phys.: Condens. Matter **16** (2004) 4455.

[16] A. A. Shokri and A. Saffarzadeh, Eur. Phys. J. B **42** (2004) 187.

[17] S. K. Watson, R. M. Potok, C. M. Marcus, V. Umansky, Phys. Rev. Lett. **91** (2003) 258301.

[18] E. R. Mucciolo, C. Chamon, C. M. Marcus, Phys. Rev. Lett. **89** (2002) 146802.

[19] B. Wang, J. Wang, H. Guo, Phys. Rev. B **67** (2003) 092408.

[20] T. Chakraborty, *Quantum Dots: A Survey of the Properties of Artificial Atoms*, Elsevier, Amsterdam (1999).

[21] M. Mardaani and K. Esfarjani, Physica E **25** (2004) 119.

[22] M. Mardaani, A. A. Shokri, K. Esfarjani, Physica E **28** (2005) 150.

[23] A. A. Shokri, M. mardaani, K. Esfarjani, Physica E **27** (2005) 325.

[24] C. Pacher and E. Gornik, Physica E **21** (2004) 783.

[25] C. Pacher and E. Gornik, Phys. Rev. B **68** (2003) 155319.

[26] J. Heinrichs, J.Phys.: Condens. Matter **12** (2002) 5565.

[27] A. F. Sadreev and I. Rotter, J. Phys.: Condens. Matter **16** (2004) 313.

[28] S. Chattopadhyay and A. Chakroborty, J. Phys.: Condens. Matter **16** (2004) 313.

[29] R. Landauer, Phys. Lett. **85** A (1986) 91.

[30] M. Büttiker, IBM J. Res. Dev. **32** (1988) 317.

[31] S. K. Maiti, J. Nanosci. Nanotechnol. **8** (2008) 4096.

[32] S. K. Maiti, Physica E **40** (2008) 2730.

[33] S. K. Maiti, Physica E **41** (2009) 1439.

[34] S. K. Maiti, J. Comput. Theor. Nanosci. **6** (2009) 1561.

[35] S. Datta, *Electronic transport in mesoscopic systems*, Cambridge University Press, Cambridge (1997).